Aus dem Institut für Pharmakologie und Toxikologie

(Professor Doktor W.-H. Zimmermann)

der Medizinischen Fakultät der Georg-August-Universität Göttingen

Characterization Of Pirfenidone Effects In Human Cardiac Fibroblasts

INAUGURAL-DISSERTATION

zur Erlangung des Doktorgrades

der Medizinischen Fakultät der Georg-August-Universität Göttingen

vorgelegt von

Friederike Elisabeth Ugi Meyer

aus Göttingen

Göttingen 2022

Dekan:	Prof. Dr. med. W. Brück

Betreuungsausschuss:

Betreuer/in:	Prof. Dr. rer. nat. S. Lutz
Ko-Betreuer/in:	Prof. Dr. rer. nat. I. Bogeski

Prüfungskommission

Referent/in:	Prof. Dr. rer. nat. S. Lutz
Ko-Referent/in:	Prof. Dr. rer. nat. I. Bogeski
Drittreferent/in:	Prof. Dr. Thomas Meyer
Datum der mündlichen Prüfung:	04.04.2024

Hiermit erkläre ich, die Dissertation mit dem Titel „Characterization Of Pirfenidone Effects In Human Cardiac Fibroblasts" eigenständig angefertigt und keine anderen als die von mir angegebenen Quellen und Hilfsmittel verwendet zu haben.

Göttingen, den …… ……

(Unterschrift)

Table of contents

II. List of figures

III. List of tables

IV. List of abbreviations

α-SMA	α-smooth muscle actin
ACE	angiotensin converting enzyme
APS	ammonium persulfate
BSA	bovine serum albumin
cpYFP	circularly permuted yellow fluorescent protein
CREB protein	cAMP-response element binding protein
CSA	cross-sectional area
CTGF	connective tissue growth factor
ddH_2O	double-distilled water
DMEM	Dulbecco's modified eagle medium
DMSO	dimethyl sulfoxide
DPBS	Dulbecco's phosphate-buffered saline
ECM	extracellular matrix
EHT	engineered heart tissue
ECT	engineered connective tissue
ERK1/2	extracellular signal-regulated kinases 1/2
FACS	flow cytometry cell cycle analysis
FBS	fetal bovine serum
FCS	fetal calf serum
FGM-3	fibroblast growth medium-3
FRET	fluorescence resonance energy transfer
hCF	human cardiac fibroblast
ECT	human engineered connective tissue
HFpEF	heart failure with preserved ejection fraction
HFrEF	heart failure with reduced ejection fraction
IPF	idiopathic pulmonary fibrosis
IL	interleukin
JNK1/2	C-Jun N-terminal kinases 1/2
LAP	latency-associated peptide
LLC	large latent complex

LTBP	latent TGF-β binding-protein
MAPK	mitogen-activated protein kinase
MEKK1	mitogen-activated protein kinase kinase kinase-1
MMPs	matrix metalloproteinases
MF	myofibroblasts
NCHF	normal human cardiac fibroblast
Pen/Strep	penicillin/streptomycin
PFA	paraformaldehyde
p38	p38 mitogen-activated protein kinase
Ras	rat sarcoma GTPase
RhoA	Ras homolog family, member A
ROCK	Rho-associated, coiled-coil-containing protein kinase
ROS	reactive oxygen species
SBE	SMAD binding element
SDS	sodium dodecyl sulfate
SDS-PAGE	sodium dodecyl sulphate-polyacrylamide gel electrophoresis
TAK1	TGF-β activated kinase-1
TBS	tris-buffered saline
TBST-T	tris-buffered saline with tween-20
TEMED	tetramethylethylenediamine
TGF-β	transforming growth factor-β
TGF-βRI/TGF-βRII	transforming growth factor-β receptor I/II
Tris	trishydroxymethylaminomethane
TRITC	tetramethylrhodamine isothiocyanate
v/v	volume percent
WGA	wheat germ agglutinine
w/o	without
2D	two-dimensional
3D	three-dimensional

1. Introduction

1.1 Cardiac fibrosis and heart failure

Fibrosis is a condition, which is defined by the over-accumulation of extracellular matrix components, such as collagen or fibronectin. It is mostly observed in injured or damaged tissues, where it leads to inflammation, dysfunction and, eventually, organ failure. Other reasons for fibrotic remodeling are chronic diseases, such as scleroderma or idiopathic pulmonary fibrosis, but also the physiological aging processes promote matrix deposition and fibrogenesis (Lopez-de la Mora et al. 2015).

In heart disease, fibrosis is characterized by the deposition of proteins increasing the fraction of extracellular matrix (ECM) in the myocardium. In fact, fibrosis is a component of almost every pathological cardiac condition. After myocardial infarction, it is mostly observed as a replacement fibrosis. The sudden loss of a substantial number of cardiomyocytes results in the release of inflammatory mediators and the activation of cardiac fibroblasts, which secrete inflammatory chemokines and cytokines. This initial inflammatory phase is dominated by the activation of the immune system, followed by the invasion of leukocytes. As the heart muscle has a very low capacity for regeneration, the following cellular key events are the proliferation of the activated fibroblasts and later on, the transdifferentiation of these cells into myofibroblasts. The latter represent the main effector cells during scar formation. This fibrotic remodeling helps to preserve the myocardial structure and prevents ventricular rupture, but it lacks the complete reestablishment of the previous contractile efficiency. The last phase, the maturation, is characterized by the cross-linking of the extracellular matrix proteins and the apoptosis of mostly all myofibroblasts in the scar. Whilst in the infarct border zone, myofibroblasts stay activated, because of volume or pressure overload, the myocardium remains in a remodeling state. Due to what is commonly referred as "reactive fibrosis", also healthy heart tissue remote from the injury site shows enhanced ECM protein production through myofibroblasts. During the tissue replacement also anti-fibrotic signals, like the expression of proteases, take place, which are supposed to counteract excessive scarring. Which exact mechanisms or signaling pathways are responsible for the observed dysbalance of extracellular matrix production and degradation, as it occurs in cardiac fibrosis, is still unknown (Kong et al. 2014; Travers et al. 2016).

Cardiac fibrosis is however not limited to occur in response to sudden events. Upon chronic stress, like constant pressure overload induced by hypertension or aortic stenosis, reactive

interstitial fibrosis can occur in the heart independent of cardiomyocytes death (Espeland et al. 2018). Whereas the level of inflammatory reaction is lower, the release of hormones and growth factors leads to an induction of crucial fibrotic and hypertrophic pathways. The gradual embedment of ECM in the myocardium can result in diastolic dysfunction, caused by insufficient relaxation. Moreover, the remodelling increases the stiffness, impedes contraction and the mechano-electric coupling, which elevates the risk for both, systolic dysfunction and arrhythmias (Ma et al. 2018).

In contrast, volume-overload, for instance as a result of valvular regurgitations or through the arteriovenous shunt in haemodialysis patients, leads to a significant loss of interstitial collagen and upregulation of matrix-metalloproteinases. Eventually, the dilatation favours the development of a systolic dysfunction and ultimately heart failure (Kong et al. 2014; Okamura et al. 2019).

Although most of the exact mechanisms causing cardiac fibrosis are still unknown and the pathological settings differ between the patients, the effector pathways seem to be similar and promote possible targets for the development of urgently needed new therapeutic strategies (Kong et al. 2014).

1.2 The role of cardiac fibroblasts

The myocardium of the adult mammalian heart is mostly anisotropic with contractile cardiomyocytes, arranged in a network of layers, electrically coupled and surrounded by extracellular matrix proteins. The dominant matrix components are collagen type I and III, and glycosaminogylcans to maintain tensile strength and elasticity at the same time (Kong et al. 2014).

Adjacent to the cardiomyocyte, many different cells, like fibroblasts, endothelial cells, leukocytes, smooth muscle cells or pericytes can be found in the heart, too. Older studies suggested that the most abundant non-myocyte cells in the myocardium are cardiac fibroblasts, however, newer findings estimated that they comprise only around 15% of all cells in the ventricular parts and up to 25% in the atrial region (Litviňuková et al. 2020). Cardiac fibroblasts can adopt diverse phenotypes and different cellular characteristics, depending on their developmental stage and environment. Due to their heterogeneity, we still lack a specific marker and therefore the knowledge about their origin, homeostasis, gene expression, and further roles in the physiological heart is still rudimental. Potential features may consist of mediating the cardiomyocyte electrical coupling or vascular maintenance (Ivey and Tallquist 2016; Rog-Zielinska et al. 2016).

However, it is common sense that the resident cardiac fibroblasts play a crucial role in maintaining the physiological myocardial structure by regulating the composition and homeostasis of the ECM (Tallquist and Molkentin 2017). Moreover, the resident cardiac fibroblasts are considered as the key source for myofibroblasts and thus the major drivers of cardiac fibrosis. The contribution of several other cell types, like bone marrow-derived progenitor cells, circulating fibrocytes, endothelial cells, epicardial cells, and pericytes may be significant, but less pronounced and seem to depend on the pathophysiologic cause and the intensity of inflammation (Kong et al. 2014; Moore-Morris et al. 2014; Ivey und Tallquist 2016; Travers et al. 2016).

In the injured heart, the resident cardiac fibroblasts are activated through the release of different cytokines and neurohumoral factors. Whereas the replacement fibrosis seems mostly driven by inflammatory cues and reactive oxygen species; mechanical stress, the activation of the renin-angiotensin-aldosterone system, and growth factors like tissue-growth-factor-β (TGF-β) are part of both, replacement and reactive interstitial fibrosis (González et al. 2018).

Activated cardiac fibroblasts proliferate more rapidly and start to express new matricellular-related genes, like periostin. Later, some of the activated cardiac fibroblasts transform into myofibroblasts, which are defined by the *de novo*-expression of α-smooth muscle actin (α-SMA) (Tallquist and Molkentin 2017). This actin isoform is necessary to produce contractile fibres, which allow the cells to exert traction forces to the ECM and thus to promote wound closer.

Beside their typical expression of α-SMA and Periostin, cardiac myofibroblasts show different morphological characteristics, like increased cytoplasm or highly developed endoplasmic reticulum and Golgi complex, as a sign of their elevated protein secretion (Ivey and Tallquist 2016). Furthermore, cardiac myofibroblasts enhance the inflammatory response by promoting the invasion of immune cells. They also show changes in the expression of adhesion molecules, like integrins, and an increase in mitochondria and respiration. Through the secretion of matrix metalloproteinases (MMPs), they empower the migration and proliferation of activated fibroblasts. Due to their highly elevated secretion of collagen I and other ECM proteins, myofibroblasts contribute to the development of excessive fibrogenesis, resulting in cardiac dysfunction (Rog-Zielinska et al. 2016; Travers et al. 2016).

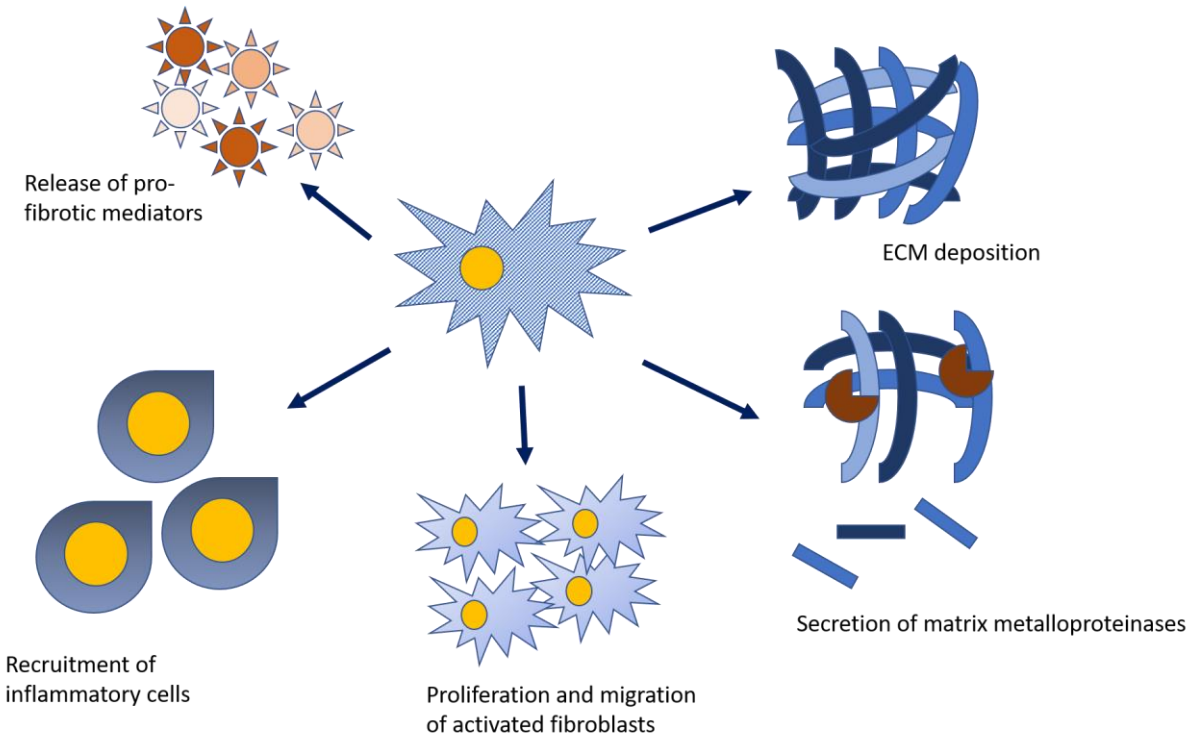

Figure 1: Schematic overview of different functions of myofibroblasts. Myofibroblasts enhance the pro-fibrotic response through various mechanisms (adapted from Travers et al. 2016)

1.3 The TGF-β signalling pathway

Amongst the known pro-fibrotic molecules, TGF-β might be one of the most important ones. Several studies have proven the increased levels of TGF-β in cardiac fibrosis (Kuwahara et al. 2002; Xiao and Zhang 2008; Kong et al. 2014), and it has been shown that in TGF-β overexpressing mice the fractional area of cardiac fibroblasts was elevated, and a significant interstitial fibrosis of the left ventricle was observed (Rosenkranz et al. 2002; Ma et al. 2018). Although, undoubtedly being pro-fibrotic in nature, the role of TGF-β in cardiac diseases seems to be double faced. It was shown that the blockade of TGF-β signalling in mice with a pressure-overload heart condition resulted not only in reduced interstitial fibrosis, but also in enhanced left ventricular dilatation and cardiac dysfunction. Moreover, in models of myocardial infarction an inhibition of the TGF-β pathway attenuated the capacity of functional and structural adaptation (Lucas et al. 2010; Ma et al. 2018).

Under healthy conditions, TGF-β is translated as a pro-peptide containing TGF-β and the latency-associated peptide (LAP). In the endoplasmic reticulum, the pro-TGF-β dimerizes and is linked to the latent-TGF-β-binding protein (LTBP) via disulphide bonds between the LAP and the LTBP. Further processing in the *trans*-Golgi network changes the interaction between TGF-β and the LAP to a still strong but non-covalent binding. Subsequently, the LTBP not

only promotes the correct folding and secretion of the pro-TGF-β through chaperone-like qualities, but also connects the tripartite large latent complex (LLC) to the ECM by possessing two ECM-binding regions. Located on the cell surface, the latent TGF-β complex works as a sensor for damage of the ECM and can be triggered through an abundance of signals like extreme pH or the release of proteases like MMPs or plasmin, eventually leading to a structural change of the LAP and the release of active TGF-β (Robertson and Rifkin 2016).

Even increased mechanical forces in the heart can contribute to the release of active TGF-β. Whereas normal soft tissue can deform under applied strain, the large latent complex stays unaffected, but, under fibrotic conditions and reduced ECM deformation, the anchorage is disturbed and active TGF-β is released (Yong et al. 2015). Additionally, local mediators like reactive oxygen species (ROS) enhance the secretion of latent TGF-β synthesized by parenchymal cell, leukocytes and platelets. Three TGF-β isoforms were identified so far, but it seems like the TGF-β1 is the predominant molecule in the heart (Pohlers et al. 2009; Ma et al. 2018).

There are two membrane-bound heterotrimeric receptors: TGFβRI and TGFβRII. Activation of the type II receptor by an active TGF-β dimer leads to the phosphorylation of TGFβRI. Consecutively, signalling molecules called SMAD2 and SMAD3 (R-SMADs) are activated through phosphorylation and released from the receptors. They bind to SMAD4 (co-SMAD) and enter the nucleus as a heterotrimeric complex. The complex interacts with specific co-activators like cAMP-response-binding protein (CREB-protein) or p300 to enhance or attenuate the expression level of different target genes to support the establishment of a profibrotic environment (Lucas et al. 2010; Kong et al. 2018; Ma et al. 2018).

For instance, the proximal promotor of the α-SMA gene possesses at least two SMAD binding elements (SBE). Especially, the initial phase in the cellular response to TGF-β seems to be driven by SMADs. Whereas crosstalk between TGF-β and other pathways like Wnt or Hippo leads to prolonged effects onto myofibroblast differentiation and ECM deposition (Carthy 2018).

Besides the SMAD-mediated canonical signalling, TGF-β also acts through non-canonical pathways including mitogen-activated protein kinases (MAPKs) and other regulatory molecules, like Ras, Raf, ERK1/2, p38 and JNK1/2. Activation of these pathways can either lead to SMAD phosphorylation, like MEKK1 promotes phosphorylation of SMAD2; or to the induction of SMAD-unrelated effects. However, they all contribute ultimately to the transcription of pro-fibrotic genes and myofibroblasts differentiation (Derynck und Zhang 2003; Pohlers et al. 2009; Travers et al. 2016).

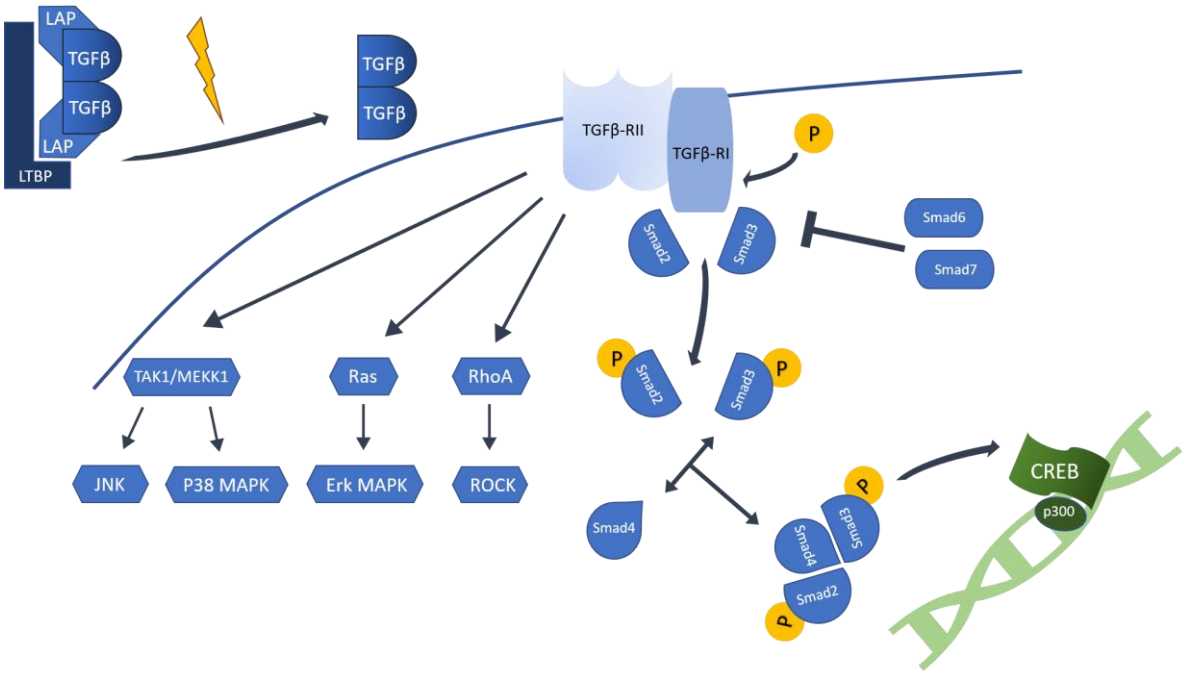

Figure 2: TGF-β signalling. The latent TGF-β- complex is anchored in the ECM via the latent-TGF-β-binding protein. Mechanical or molecular changes lead to a structural change of the latency-associated peptide and the release of active TGF-β dimers. Activation of the TGF-β receptors (TGF-βRII and TGF-βRI) results in canonical signalling via SMADs and nuclear co-activators, like cAMP-response element binding protein (CREB) or p300. Activation of non-canonical pathways include mitogen-activated protein kinases (MAPK) and different mediators like Ras (rat sarcoma GTPase), ERK1/2 (extracellular-signal regulated kinases 1/2), TAK1/MEKK1 (TGF-β activated kinase-1/ mitogen-activated protein kinase kinase kinase-1), p38 (p38 mitogen-activated protein kinase), JNK1/2 (c-Jun N-terminal kinases 1/2), RhoA (Ras homolog family, member A), and ROCK (rho-associated, coiled-coil-containing protein kinase). (adapted from Pohlers et al. 2009)

1.4 Engineered connective tissue as an *in vitro* 3D-model

Apart from molecular pathways, also biomechanical cues like enhanced extracellular matrix stiffness, disturbed cyclic stretch and other abnormal applied forces are known to activate the transdifferentiation of cardiac fibroblasts into myofibroblasts. In the pressure-overloaded heart, cardiac fibroblasts are subjected to an increased strain (relative deformation) and enhanced stress (force per unit area), leading to the release of pro-fibrotic mediators, followed by the activation of crucial pathways and eventually fibrotic remodelling, which contributes to myocardial stiffness and intensified myofibroblast differentiation. Thus, it can be assumed that cardiac (myo)fibroblasts are in fact self-reinforcing their own generation by creating a stiff environment (Yong et al. 2015; Cho et al. 2018).

The cell's ability to sense the mechanical properties of their surroundings, and accordingly change their morphology, is called mechanotransduction. The main mediators are cell-ECM and cell-cell contacts, like integrin-containing focal adhesions and cadherin-based adherens junctions, which transfer extracellular physical stress to intracellular signalling pathways. These processes play an important role in the physiological as well as the injured heart and could be part of reactive and repair mechanisms to direct the cells migration (Solon et al. 2007; Sadeghi et al. 2017).

Unfortunately, it occurs that merely culturing cardiac fibroblasts in two-dimensional (2D) plates provokes the same matrix-induced behaviour through spontaneous activation (Sadeghi et al. 2017; Baranyi et al. 2019). Therefore, multiple studies have investigated the effects of growing cardiac fibroblasts in matrices with tuneable stiffness. They showed that cardiac fibroblasts adapt their internal stiffness to their environment by changing their cytoskeletal structure and by the formation of cell-matrix contacts. In high tension models, like commonly used glass or plastic coverslips, the production of actin stress fibres, upregulation of focal adhesions, and the development of a more spread morphology were observed, eventually resulting in a myofibroblast phenotype (Rhee and Grinnell 2007; Solon et al. 2007). Besides structural effects, it has also been shown that in a stiff environment proliferation was increased and cell cycle analyses revealed an increased proportion of cells in S-phase. In line, DNA synthesis was enhanced on stiff surfaces (Qiu et al. 2015). Moreover, in a 2D model of polyethylene glycol hydrogel-based ECM with patterned stiffness, cardiac fibroblasts were migrating to the stiff area and transdifferentiated there into myofibroblasts (Yong et al. 2015).

Whereas most of the studies on cardiac (myo)fibroblast behaviour were carried out in 2D cultures, there is a lack of exploring their behaviour in a more physiologically relevant three-dimensional (3D) setting. Especially when it comes to the analysis of mechanical features and the influence of changes in the ECM, 2D models are not sufficient to allow reliable conclusions about possible *in vivo* effects. The heart muscle, for example, has an elastic modulus of 18kPa whereas the stiffness of 2D culture plastic dishes is in the range of gigapascal (Xie et al. 2014; Bracco Gartner et al. 2019). To face these deficits, engineered tissues were developed as promising drug screening and disease models. Proving the benefits of engineered tissues as a more *in vivo*-like setting, Bracco Gartner et al. (2019) showed that cardiac fibroblasts were in fact more quiescent when cultured in a 3D hydrogel model with a heart-like elastic modulus. Whereas Galie et al. (2011) proved that in 3D-collagen matrices a higher stiffness promoted the differentiation into a myofibroblast phenotype.

Different techniques to generate engineered connective tissue (ECT) were developed throughout the years, whereas the currently most used system contains a hydrogel (usually

collagen I) mixed with cells in a casting mould including a mechanical support (Weinberger et al. 2017; Zuppinger 2019). Over the last decades, fibroblast-populated collagen gels turned out to be a versatile tool to investigate mechanical and biological tissue characteristics. Prior studies mostly focused on measuring cell traction force parameters and in the establishment of a consistent model (Barocas et al. 1995). Soon, further investigations used the model to analyse tissue properties, like stiffness and force regulation. As these engineered connective tissues (ECT) provided insights in cell-ECM interactions, cell motility, collagen remodelling, and contractility, one of the main subjects was the characterization of connective tissue development and wound repair (Eastwood et al. 1996; Wakatsuki et al. 2000; Dallon and Ehrlich 2008; Toki et al. 2013). Additionally, Chan et al. (2010) introduced a method to measure the cellular response to mechanical forces by analysing alterations on gene expression, like the regulation of the α-SMA promotor. Whereas Chao et al. (2015) studied the induction of regulatory proteins like the monocyte chemotactic protein-induced protein 1 in fibroblast populated 3D collagen matrices.

One of the advantages of a single cell-based tissue model is the possible specification of the composition to address certain pathways, for instance by using cytochalasin D to evaluate the impact of a disrupted actin cytoskeleton on cell stiffness and contraction (Wakatsuki et al. 2000). Furthermore, cell density and ECM components can be adjusted depending on the experimental setting and mechanical tests can be used to reveal changes in viscoelasticity and contractility (Elson and Genin 2016).

Taken together, these benefits strongly indicate that ECT models unite the necessary properties to represent the optimal drug testing tool. Therefore, this model was chosen as it offers a new approach to investigate how promising drugs interfere with cardiac fibroblasts and their influence on the biomechanical properties of the ECM.

1.5 Current treatment of cardiac fibrosis

So far, current medical treatment is only able to decelerate the progression of cardiac fibrosis, but is still lacking a specific targeted therapy and in fact, fibrosis does not appear as a primary target in the current treatment guidelines of heart failure (Zhao et al. 2014, Gourdie et al. 2016, de Boer et al. 2019).

Consequently, no striking discoveries were made in the field of treating cardiac fibrosis for several years. So far, only angiotensin-converting-enzyme (ACE) inhibitors, aldosterone antagonists, angiotensin receptor blockers, and statins are known to have beneficial effects to delay the progression of the fibrotic remodelling towards heart failure (Gourdie et al. 2016). Other conventionally used drugs like β-blockers had anti-fibrotic effects in animal models and

are associated with positive long-term outcomes in patients with heart failure in question of all-cause mortality. However, whether they are influencing the progress of fibrogenesis is still unknown (Fang et al. 2017).

Most of the drugs have shown their benefits only in patients with heart failure with reduced ejection fraction (HFrEF). For patients with heart failure with preserved ejection fraction (HFpEF) or other forms of cardiac fibrosis, no notable effects were observed, so far (Park et al. 2019). Furthermore, studies indeed proved that ACE inhibitors and angiotensin receptor blockers are capable to reduce cardiac fibrosis, but only in a modest range and in patients with severe heart failure, cardiac fibrosis persisted even when treated as recommended by the guidelines. Another problem is that the current guidelines do not discriminate between the different pathological causes of the fibrotic process, which results in contrary outcomes in various studies, hindering the translation into clinical settings. These findings strongly indicate the need to develop novel and specific treatment strategies in fibrotic heart diseases (Fang et al. 2017; de Boer et al. 2019).

One problem in finding new therapeutic options is that the fibrotic remodelling cannot be blocked entirely as it is an important part of the tissue replacement to prevent cardiac rupture, since cardiomyocytes are limited in their proliferation to fully replace the damaged muscle (Park et al. 2019).

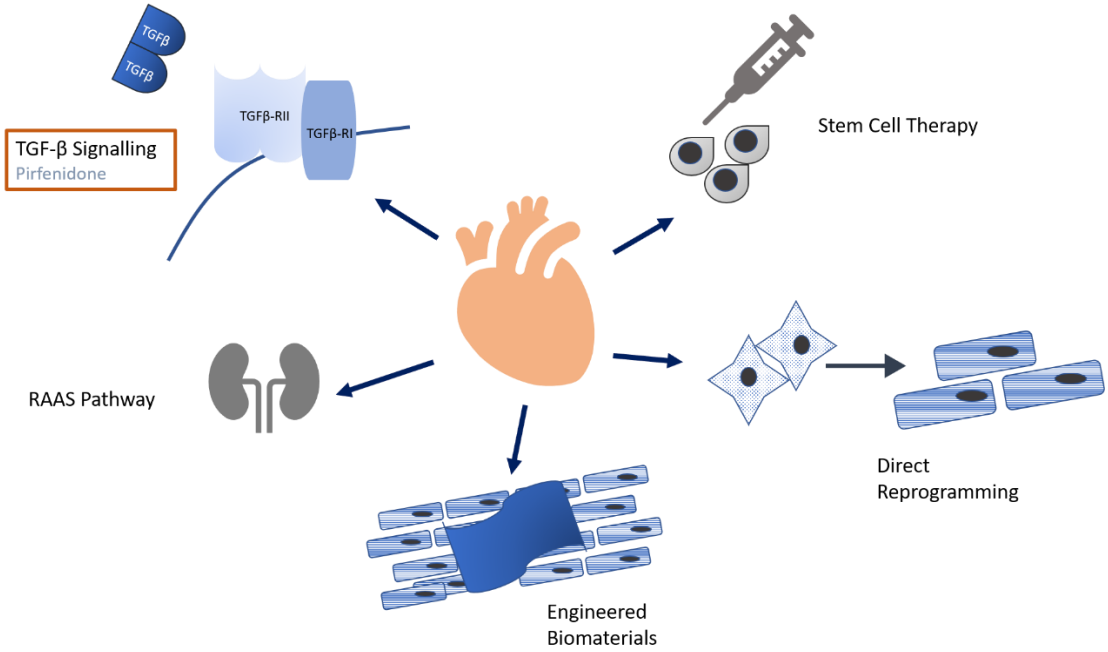

Figure 3: Potential therapeutic targets in treating cardiac fibrosis. Current approaches for specific anti-fibrotic therapies include the search for new mediators in crucial signalling pathways, like TGF-β or the renin-angiotensin-aldosterone system (RAAS), together with direct cellular replacement

New approaches focus on the inhibition of known fibrotic pathways like TGF-β-, angiotensin II, or endothelin signalling. Chen et al. (2019) just discovered the role of the E3 ubiquitin ligase WWP2 as a part of pro-fibrotic TGF-β signalling and SMAD2 regulation, making it an attractive object for drug development. Additionally, other recently identified mediators, like Relaxin-2, certain miRNAs, or cardiotrophin-1, are now tested as potential therapeutic targets. Further studies investigated the effects of reducing the inflammatory response, for instance by generating monoclonal antibodies against the monocyte chemoattractant protein-1 (MCP-1) or a specific inhibitor against the chymotrypsin-like serine protease chymase that is released from mast cells by increased inflammation and plays a key role in the local renin-angiotensin system (Oyamada et al. 2011; Gourdie et al. 2016).

Another upcoming field lays in cell-based approaches, like the application of engineered biomaterials or reprogramming cardiac fibroblasts into cardiomyocytes. In addition, future therapeutic strategies may include the use of stem cells to regenerate cardiomyocytes or the stimulation of cardiac progenitor cells to replace the injured myocardium. However, facing the complexity of cardiac fibrosis a possible solution may lay in the combination of multiple therapies (Gourdie et al. 2016; Fang et al. 2017; Park et al. 2019).

1.6 Pirfenidone as a promising anti-fibrotic drug

Pirfenidone is small synthetic pyridine molecule, which was shown to have anti-fibrotic, anti-inflammatory, and antioxidant effects in pre-clinical settings. Hitherto, most of these effects seem to be carried out by inhibiting TGF-β signalling, although the exact target remains unknown (Graziani et al. 2018; Park et al. 2019).

The anti-fibrotic properties of pirfenidone were firstly described in 1995 in a rodent model of bleomycin-induced lung fibrosis. Afterwards, these beneficial effects were further investigated and reproduced multiple times in different animal models of fibrotic diseases (Shi Q et al. 2011). With respect to cardiac fibrosis, it was shown that pirfenidone reduced the ventricular remodelling, improved cardiac hypertrophy, and increased the overall survival in a murine model of pressure overload-induced heart failure (Graziani et al. 2018; Park et al. 2019; Aimo et al. 2020). In a rat model of hypertension, a two-week pirfenidone treatment attenuated the development of cardiac fibrosis and perpetuated the diastolic function. In another mouse model of pressure-overload induced by transverse aortic constriction, pirfenidone successfully reduced hypertrophy and inflammation in the left ventricle, whereas no effects on the blood pressure were observed. So far, Pirfenidone did not show any haemodynamic effects at all (Lewis et al. 2019; Aimo et al. 2020).

Additionally, in myocardial infarction rat models, cardiac scarring and remodelling in the border zone were attenuated and the development of cardiac dysfunction was decelerated after pirfenidone treatment. In a dog model with heart failure induced by high frequency left ventricular pacing, pirfenidone prevented left atrial fibrosis and therefore lowered the risk for atrial fibrillation (Graziani et al. 2018; Park et al. 2019; Aimo et al. 2020). Another study of rats, receiving doxorubicin injections for two weeks, showed that the pirfenidone-treated rats had a lower mortality rate, reduced heart weight, and less histopathological changes (Lewis et al. 2019; Aimo et al. 2020). Furthermore, molecular pathways and changes on cellular levels were investigated and revealed that pirfenidone inhibits TGF-β transcription and downstream TGF-β signalling pathways (Park et al. 2019). One of the most prior studies of pirfenidone described the suppression of bleomycin-induced TGF-β overexpression in a hamster bleomycin model (Iyer et al. 1999). In human alveolar epithelial cells, pirfenidone inhibited the TGF-β stimulated collagen type I expression (Hisatomi et al. 2012). Suitably, pirfenidone decreased the TGF-β-stimulated collagen synthesis and reduced proliferation and myofibroblast transdifferentiation in human lung fibroblasts (Graziani et al. 2018). The same effects were observed in cardiac fibroblasts and additionally, pirfenidone-treatment reduced α-smooth muscle actin expression and consequently stress fibre formation in 2D cultures. It further rebalanced the ratio of MMPs and tissue inhibitors of metalloproteinases. In 3D, pirfenidone prevented the myofibroblast driven contraction of free-floating collagen-cell discs (Shi X et al. 2011). Other pro-fibrotic and inflammatory mediators, like fibrogenic growth factors, interleukin (IL) 1β, IL-4 and IL-13, were suppressed in several studies after pirfenidone treatment and furthermore, the formation of the NLRP3 inflammasome seemed to be reduced, too. Moreover, even the immune system, especially T- and B-lymphocyte activity might be influenced by the presence of pirfenidone, although no exact mechanisms were discovered, so far (Aimo et al. 2020).

Another approach how pirfenidone may counter fibrogenesis may be trough the reduction of reactive oxygen species (ROS). In a rodent animal model pirfenidone was able to reduce the production of ROS in cardiomyocytes under basal conditions and in the presence of pro-oxidants like hydrogen peroxide. After an exposure time of 30 min with hydrogen peroxide, ROS production in pirfenidone-treated cells was lowered compared to control (Monsalvo-Villegas et al. 2018). Additionally, pirfenidone was able to reduce circulating markers of oxidative stress, perhaps through interactions with the membrane potential in mitochondria (Aimo et al. 2020). When mixed with iron chloride, pirfenidone forms a stable pirfenidone-iron complex that is known to have superoxide scavenging activity and inhibits the Fenton reaction. Its chelating constant leads to the assumption that these complexes are likely to appear in

biological systems and may partly explain the anti-fibrotic effects of pirfenidone (Mitani et al. 2008).

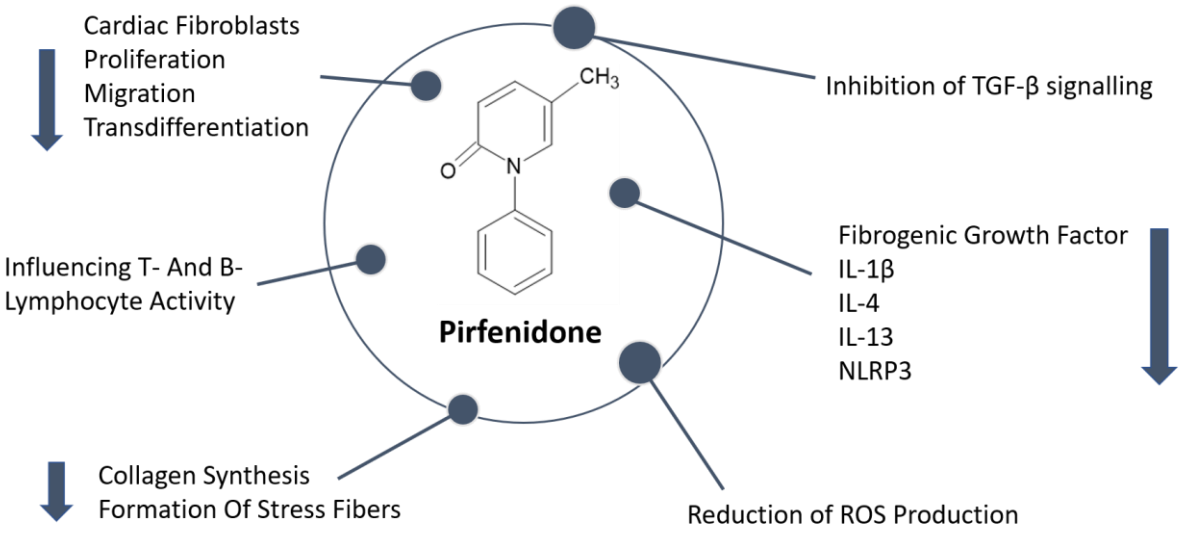

Figure 4: Proclaimed effects of pirfenidone.

After this broad range of convincing results about its anti-fibrotic effectiveness in pre-clinical trials, pirfenidone was first approved for the treatment of idiopathic pulmonary fibrosis (IPF) in 2008 in Japan (Pirespa®). In 2011 and in 2014 the European Union (Esbriet®) and the U.S. Food and Drug Administration authorized the usage of pirfenidone for treating IPF, too (Ogura et al. 2015; Lewis et al. 2019; Park et al. 2019).

IPF is defined as a severe, chronic, and progressive interstitial pneumonia of unknown cause. Recently, meta-analysis confirmed that pirfenidone reduces the progression of IPF in terms of forced vital capacity decline and the risk of all-cause mortality (Rogliani et al. 2016; Pan et al. 2017). The approved dosage of pirfenidone for treating IPF is 2403 mg/day separated into 267 mg capsules, taken orally three times per day (Rogliani et al. 2016; Lewis et al. 2019).

In a pharmacokinetic study in healthy Chinese volunteers orally taken pirfenidone showed a median time to maximum plasma concentration of 0.33-1 h and was cleared from plasma after 2 to 2.5 h. There was no evidence of pirfenidone accumulation after multiple doses (Shi et al. 2007). In a rat model, pirfenidone showed a bioavailability of 46%; however, so far, there is no data for humans available. Pirfenidone enters the cell by passive diffusion and can also cross the blood-brain barrier, in the plasma 60% is bound to proteins like albumin. In animal models is has been shown that the majority of the drug is rapidly metabolized by various cytochrome P450 enzymes in the liver into mainly 5-carboxy-pirfenidone and additionally 5-hydroxy-pirfenidone and excreted by 80 % through the urine and 20% through the intestinal system.

Recent studies suggest additional anti-fibrotic properties of these metabolites (Ogura et al. 2015; Togami et al. 2015; Aimo et al. 2020).

Although, it is mostly well-tolerated, frequently observed mild systemic adverse effects during pirfenidone treatment are photosensitivity, anorexia, and nausea, appearing in a dose-dependent matter and less severe when the drug is taken with food (Togami et al. 2015; Pan et al. 2017). Lately, new evidence suggest that prolonged treatment may lead to hepatic toxicity and eventually liver dysfunction. Therefore, liver monitoring is strongly recommended before and periodically during treatment (Fang et al. 2017; Martinez et al. 2017; Park et al. 2019).

As the safety and efficacy as well as tolerability of pirfenidone was proven in multiple studies, it is today acknowledged as the standard-of-care approach to clinical management of IPF and further fields of application are now under intensified investigation (Meyer and Decker 2017). In fact, pulmonary and cardiac fibrosis share some important characteristics, as typical occurring changes in the diseased lung, like unregulated ECM deposition, release of pro-fibrotic and pro-inflammatory mediators, especially TGF-β, the differentiation of lung fibroblasts into myofibroblasts, and eventually, increased tissue stiffness, are also crucial changes in the remodelling heart. Taken this into account, pirfenidone is now tested in ongoing trials as a promising new therapeutic approach for the treatment of cardiac fibrosis (Meyer and Decker 2017; Aimo et al. 2020).

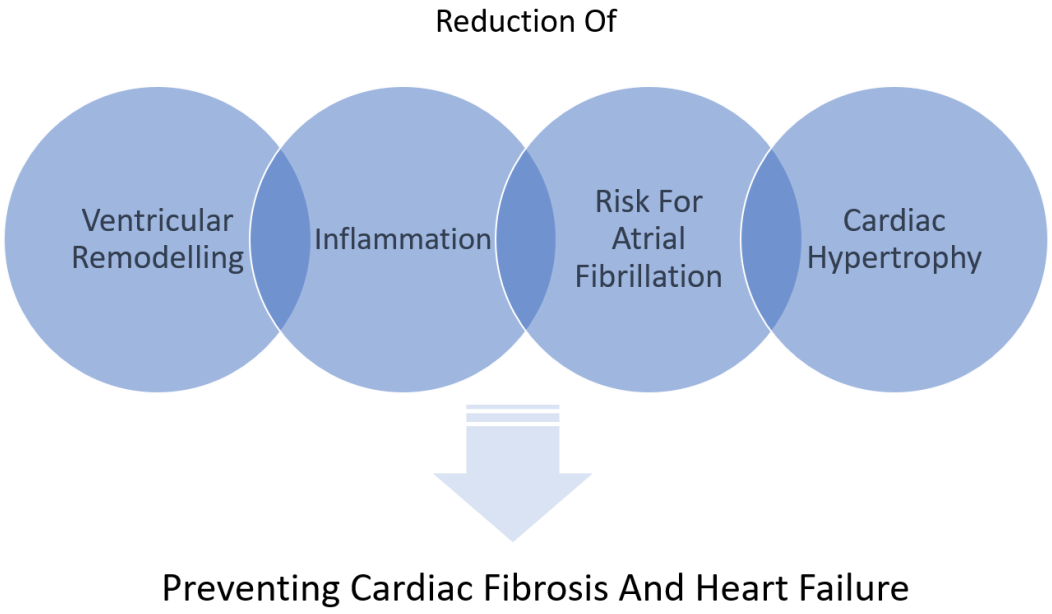

Figure 5: Outcome of pirfenidone actions possibly resulting in the reduced risk of cardiac fibrosis and heart failure.

To evaluate the effects of pirfenidone on myocardial fibrosis in patients, the PIROUETTE (PIRfenidOne in patients with heart failure and preserved lEfT ventricular Ejection fraction) trial was designed as a randomised, double-blinded, placebo-controlled phase 2 study. The included patients were suffering from chronic HFpEF and myocardial fibrosis and received 52 weeks of treatment. The active group was given pirfenidone, titrated as tolerated, over a 14-day period to the full daily dose of 2403 mg, in 267mg capsules three times a day (Lewis et al. 2019). First results demonstrated that after a treatment period of 52 weeks, a reduction of the myocardial extracellular volume in the pirfenidone group was observed. Although the effect was rather small (between-group difference, −1.21%; 95% confidence interval, −2.12 to −0.31; P = 0.009,) it was still significant and met the predefined primary outcome (Aimo et al. 2021; Lewis et al. 2021).

Further ongoing studies are investigating the impact of pirfenidone in other organs. For instance, an open-label, single-centre pilot study of pirfenidone effects on focal segmental glomerulosclerosis and a randomized, placebo-controlled clinical study on diabetic nephropathy already showed some promising results (Graziani et al. 2018).

1.7 Intracellular H_2O_2 measurements using the genetically encoded sensor HyPer

Oxidative stress is known to play an important role in the development of fibrotic remodelling. Elevated ROS production results in non-specific oxidation of proteins, lipids, or DNA, and eventually in cellular dysfunction. As antioxidant properties of pirfenidone were already described in several studies, one aim of this project was to evaluate how pirfenidone is able to influence the redox status of cells under basal conditions and in the presence of strong oxidants. Therefore, H_2O_2 was chosen, as it is a well-studied ROS and important second messenger that mainly regulates protein activity by modifying their thiol residues.

To monitor the redox-level in cells, a genetically encoded and highly specific fluorescent detector for H_2O_2 was used. The sensor was developed by inserting a circularly permuted yellow fluorescent protein (cpYFP) into the regulatory domain of the H_2O_2-sensing protein named OxyR. Circularly permuted fluorescent proteins are highly sensitive to the conformation of a protein and can produce a fluorescent signal depending on their environment. OxyR is a protein, found in *Escherichia coli* and consists of two domains, one H_2O_2-sensitive regulatory domain and a DNA-binding domain. The regulatory domain contains two important cysteine residues, Cys199 and Cys208. The first one is normally located in a hydrophobic pocket, which can be reached by the amphiphilic H_2O_2 molecule. By oxidizing the Cys199 to a sulphenic acid

derivative, the cysteine is released from the hydrophobic pocket and gets close enough to the Cys208 to form a disulphide bond, leading to a change of the protein's conformation.
As it has a sub-micromolar affinity to H_2O_2, but an insensitivity to other oxidants at the same time, HyPer possesses some advantages compared to other sensors. Belousov et al. showed that HyPer is a utile instrument to measure changes in the H_2O_2 concentration in cytoplasm and mitochondria at single cell level. The intracellular changes can be tracked in real-time as an oxidation leads to a shift of the excitation peaks of the attached cpYFP, represented by an increase at 500nm and a decrease at 420 nm. In the reducing environment of the cytoplasm changes are rapidly reversible, resulting in a dynamic monitoring of the cellular redox state. As a molecular probe, HyPer can be transfected into specific cells and even targeted to different organelles (Belousov et al. 2006; Niethammer et al. 2009; Markvicheva et al. 2011; Hernández-Barrera et al. 2013).

1.8 Aims

Cardiac fibrosis represents a major problem in heart diseases, while it is still lacking an effective therapy. Though, cardiac fibroblasts are identified as crucial players in the fibrotic remodelling, further investigations are still necessary to understand the underlying pathogenesis and detect possible targets for new therapeutic approaches.
Since the novel drug pirfenidone showed impressive anti-fibrotic effects in animal models of heart diseases, the aim of this study was to investigate how pirfenidone is affecting the behaviour of human cardiac fibroblasts.
As the first part of the project, pirfenidone effects in 2D-cultured human cardiac fibroblasts were studied to assess influences on proliferation, viability and cell signalling. Afterwards, ECT were used as a model for drug screening to detect how pirfenidone is affecting the cellular behaviour and biomechanical properties, like compaction, contraction, and stiffness. The third aim was to determine antioxidant capacities of pirfenidone by real-time monitoring the H_2O_2 concentration in living cells using the fluorescent biosensor HyPer.

2. Materials and Methods

2.1 Cells

Normal human cardiac fibroblasts (ventricle, male donor), Lot No.: 0000421712, Lonza

tsA201: Human embryonic kidney, immortalized by SV-40 large T antigen

tsA201 HyPer: Human embryonic kidney, immortalized by SV-40 large T antigen, genetically encoded fluorescent hydrogen peroxide sensor, kindly provided by I. Trautsch (Institute of Pharmacology and Toxicology, University Medical Center Göttingen, Germany)

2.2 Chemicals, reagents and consumables

Table 1: Fine chemicals and reagents

(adapted from Mügge 2018)

Reagent	**Company**
Acetic Acid	Carl Roth
Acrylamide solution rotiphorese gel 30	Carl Roth
Ammonium persulfate (APS)	Invitrogen
β-Mercaptoethanol	AppliChem
Bovine serum albumin (BSA)	Thermo Fisher Scientific
Bromophenol blue	Sigma Aldrich
Calcium chloride ($CaCl_2$)	AppliChem
cOmplete protease inhibitor cocktail tablets	Roche
Cytobuster protein extraction reagent	Merck
DAPI (4‘,6-diamidino-2-phenylindole)	Sigma Aldrich
Ethanol	Carl Roth
Glycerol	Carl Roth
Hydrochloric acid (HCl)	Carl Roth
Hydrogen Peroxide (H_2O_2) 30%	Sigma Aldrich
Isopropanol	Carl Roth
Lumi-Light^{PLUS} Western Blotting Substrate	Roche
Magnesium chloride ($MgCl_2$)	AppliChem
Methanol	Carl Roth
Paraformaldehyde (PFA)	Sigma Aldrich
PhosSTOP phosphatase inhibitor cocktail tablets	Roche

Ponceau-S	Sigma Aldrich
Potassium chloride (KCl)	Carl Roth
Propidium iodide solution	Sigma Aldrich
Protein Marker „Roti-Mark Standard“	Carl Roth
Protein Marker „Roti Mark TRICOLOR“	Carl Roth
Roti-Block (blocking reagent)	Carl Roth
Roti-Free Stripping-Puffer 2.2 plus	Carl Roth
Sodium chloride (NaCl)	Carl Roth
Sodium dodecyl sulfate (SDS)	AppliChem
Super Signal West Femto	Thermo Fisher Scientific
Tetramethylethylenediamine (TEMED)	Merck
Tris	Carl Roth
TRITC- phalloidin	Sigma Aldrich
Triton-X 100	Carl Roth
Tween-20	Carl Roth

Table 2: Consumables

Consumables	**Type**	**Company**
Casting moulds	Circular, 3 stiff poles	house-made, kindly supplied by the Institute of Pharmacology and Toxicology, University Göttingen
Cell culture flasks	T75, T25	Sarstedt
Cell culture multiwell plates	48- well, 24- well, 12- well, 6-well	Sarstedt
	48- well, with flexible rubber poles for generation of ECT	Custom-made according to patent No. 2016060314484000DE hold by the Institute of Pharmacology and Toxicology, University Göttingen
Cell culture plates	10 cm	Sarstedt

Cell scraper	1.7 cm 2-position blade	Sarstedt
Collecting tubes	15 ml, 50 ml	Cellstar
Cryotubes	1.8 ml	Thermo Fisher Scientific
Filter tips	10 µl, 100 µl, 1000 µl	Greiner Bio One
Microtest plates	96-well, F	Nunc
	96-well, U, imaging	Zell-Kontakt
Multi tips	2 ml, 5 ml, 10 ml	Eppendorf
Nitrocellulose blotting membrane	Amersham Protran 0.2 µM NC	GE Healthcare Life Science
Pasteur pipettes	230 mm	Labsolute
Pipette tips	10 µl, 100 µl, 1000 µl	Sarstedt
Pipette tips for microplate reader	96-count	Molecular Devices
Reaction vessels	0.5 ml, 1.5 ml, 2 ml	Eppendorf
Sterile serological pipettes	2 ml, 5 ml, 10 ml, 25 ml	Sarstedt

2.3 Devices

Table 3: Devices

(adapted from Hartmann 2016)

Device	**Type**	**Company**
Autoclave	VX-150	Systec
Automated multiparameter cell analysis machine	Cellavista	SynenTec
Blotting chamber	Mini Trans-Blot Cell	Bio-Rad Laboratories
Cell counter and analyzer	CASY Model TTC	Roche
Centrifuges	Centrifuge 5417R	Eppendorf
	Heraeus Megafuge 40R	Thermo Fisher Scientific
Chemiluminescence imager	ChemiDoc MO	Bio-Rad Laboratories
Digital camera	α6000	Sony
Flow Cytometer	BD LSR II	BD Biosciences
Freezing Container	Mr. Frosty	Nalgene
Gel electrophoresis chamber	Mini-PROTEAN Tetra	Bio-Rad Laboratories
Inverted light microscope	Primo Vert	Zeiss

	Axiovert 200	Zeiss
Inverted fluorescence microscope	IX81	Olympus
Microscope camera	XM10	Olympus
Microscope filter blue	350 DAPI	Olympus
Microscope filter red	575 TxRed	Olympus
Microscope filter green	485 FITC	Olympus
Microscope objective 4x	UPlanFLN4xPh	Olympus
Microscope objective 10x	UPlanFLN10xPh	Olympus
Microscope objective 20x	LUCPlanFLN20xPh	Olympus
Heating block	Thermomixer compact	Eppendorf
Heating plate magnetic	RCT basic	Janke u. Kunkel IKA Labortechnik
Incubators	C200	Labotect
Multi-mode microplate reader	FlexStation 3	Molecular Devices
pH-meter	Inolab pH	Wtw
Power supply	Power PAC HC	Bio-Rad Laboratories
Rheometer	RSA-G2	TA instruments
Scales	AX2224	Sartorius
	AZ2101	Sartorius
	R 160 P	Sartorius
Shakers	3016	GFL
	Vibramax 100	Heidolph
Sterile Hood	Herasafe 2030i	Thermo Fisher Scientific
Stereomicroscope	M80	Leica
Stereomicroscope Microscope camera Microscope objective Microscope light	Lumar.V12 AxioCam MRc Neo LumarS 0.8x FWD 80mm KL 2500 LCD	Zeiss Zeiss Zeiss Zeiss
Table Centrifuge	Centrifuge 5415D	Eppendorf
Ultra pure water system	Milli-Q	Merck
Vacuum pump	Laboport	KNF

Vortexer	VF2	Krannich
	Vortex Genie 2	Bender & Hobein AG
Water bath	Thermostat 2764	Eppendorf

2.4 Cell culture media and additives

Table 4: Additives for cell culture

Reagent	**Company**
CASYton	OLS OMNI Life Science
Collagen I (bovine) 6.49 mg/ml	Devro Pty. Ltd.
Collagenase I	Sigma Aldrich
Dimethyl sulfoxide (DMSO)	Sigma-Aldrich
DMEM (Dulbeccos modified eagle medium) powder 10x	Life Technologies
DMEM GlutaMAX ([+]4.5g/l D-Glucose; [-] Pyruvate)	Life Technologies
DNaseI stock solution	Calbiochem
DPBS (Dulbeccos phosphate buffered saline), w/o calcium and magnesium chloride	Life Technologies
Fetal bovine serum (FBS)	Life Technologies
Fibroblast growth medium-3 (FGM-3)	PromoCell
Penicillin-streptomycin (PenStrep), 100x (10000 U/ml penicillin, 10000 µg/ml streptomycin)	Life Technologies
Pirfenidone (HY-B0673)	Hycultec MedChemExpress
Puromycin (10 mg/ml)	Life Technologies
SupplementPack FGM-3 1x C-37340 FCS-50 1x C-30310 hbFGF-0.5 1x C-3101 Insulin-2.5	PromoCell
StemPro Accutase cell dissociation reagent	Millipore
Transforming-growth-factor-β1 (TGF-β1), human	PeproTech
TrypLE Express	Life Technologies

Trypsin	Gibco

Table 5: Cell culture media and solutions

tsA201 culturing	
Heat-inactivated FBS	50 ml FBS was incubated in a water bath at 56°C for 30 min
Growth medium	DMEM GlutaMAX 4.5 g/l glucose 10% FBS heat-inactivated (v/v) 1% PenStrep (v/v)
NCHF culturing	
Growth medium	500ml FGM-3 (v/v) SupplementPack FGM-3 3 (v/v) 10% FCS 0.1% hbFGF 0.5% Insulin 1% PenStrep (v/v)
Generation of human engineered connective tissue (ECT)	
2x DMEM	20% DMEM 10x (v/v) 20% FBS (v/v) 2% PenStrep (v/v) In ddH_2O, sterile, filtered

2.5 Buffers and solutions

Table 6: Buffers and solutions

Immunofluorescence	
4% PFA	40 g PFA 200 µl 10 N NaOH 100 ml 10x DPBS ddH_2O to 1000 ml pH 7.0 with HCl
0.2% Triton X-100	1 ml 10% Triton X-100 DPBS to 50 ml
1x Roti- Block	5 ml Roti- Block

	ddH_2O to 50 ml
Flow cytometry cell cycle analysis	
Blocking buffer	500 ml DPBS (w/o Ca/Mg) 27 ml FBS 5 ml BSA 2.6 ml Triton X-100
SDS-PAGE and immunoblot	
Lysis buffer	10 ml Cytobuster reagent 1 tablet cOmplete protease inhibitor cocktail 1 tablet PhosSTOP phosphatase inhibitor cocktail
4x SDS-PAGE sample buffer (Laemmli buffer)	50 ml Glycerol 10 ml β-Mercaptoethanol 3.6 g Tris 5.7 g SDS 0.2 g Bromophenol blue ddH_2O to 100 ml pH 7.4 with HCl
10% APS	1 g APS ddH_2O to 10 ml
10% SDS	10 g SDS ddH_2O to 100 ml
1 M Tris solution pH 6.8	121.14 g Tris ddH_2O to 1000 ml pH 6.8 with HCl
1.5 M Tris solution pH 8.8	181.71 g Tris ddH_2O to 1000 ml pH 8.8 with HCl
10 x SDS-PAGE running buffer	250 mM Tris 1.92 M Glycine 1% SDS pH 8.3 with HCl
1x SDS-PAGE running buffer	200 ml 10x SDS-PAGE running buffer ddH_2O to 2000 ml

1x Transfer buffer	6 g Tris 28.8 g Glycine 400 ml Methanol ddH_2O to 2000 ml pH 8.4 with HCl
10x Tris-buffered saline (TBS)	0.2 M Tris 1.5 M NaCl pH 7.4 with HCl
1x TBS with Tween-20 (TBST)	200 ml TBS 2 ml Tween-20 ddH_2O to 2000 ml
Ponceau-S solution	0.2 g Ponceau-S 3 ml Acetic acid ddH_2O to 100 ml
Intracellular H_2O_2 measurements	
FRET buffer	114 mM NaCl 5.4 mM KCl 1mM $MgCl_2$ 2 mM $CaCl_2$ 10 mM HEPES ddH_2O to 1000 ml pH 7.4 with HCl

2.6 Antibodies

2.6.1 Primary antibodies

Table 7: Primary antibodies

Primary Antibody against	Dilution	Clone/Company	Species
α-Tubulin	1:2000	Monoclonal B-5-1-2 T5168, Sigma Aldrich	Mouse
α-Smooth muscle-actin	1:2500	Monoclonal 1A4 A5228, Sigma Aldrich	Mouse
Pro-collagen I, alpha 1	1:2000	Polyclonal, 41858 Rockland	Rabbit
CTGF	1:200	Polyclonal, 14939, Santa Cruz	Goat

Periostin	1:1000	Monoclonal, 39863, Santa Cruz	Mouse
Phospho-SMAD2 (Ser465/467)	1:1000	Monoclonal, 3108S, Cell Signaling	Rabbit
Phospho-SMAD3 (Ser423/425)	1:1000	Monoclonal, C25A9, Cell Signaling	Rabbit
SMAD2	1:1000	Monoclonal, D43B4, Cell Signaling	Rabbit
SMAD3	1:1000	Monoclonal, C67H9, Cell Signaling	Rabbit
SMAD2/3	1:1000	Monoclonal, 8685S, Cell Signaling	Rabbit
PathScan Multiplex Western Cocktail I (Phospho-p90RSK, Phospho-Akt, Phospho.p44/42 MAPK, Phospho-S6 Ribosomal Protein)	1:200	Polyclonal, 5301S, Cell Signaling	Rabbit
P-p44/42 MAPK (ERK1/2)	1:2000	Monoclonal, 9101S, Cell Signaling	Rabbit
P44/42 MAPK (ERK1/2)	1:1000	Polyclonal, 9102S, Cell Signaling	Rabbit
P-MEK 1/2	1:1000	Polyclonal, 9121S, Cell Signaling	Rabbit
MEK 1/2	1:1000	Polyclonal, 9122S, Cell Signaling	Rabbit

Primary antibodies were incubated overnight at 4°C whilst shaking.

2.6.2 Secondary Antibodies

Table 8: Secondary antibodies for immunoblot analysis

Secondary antibody against	Dilution	Company	Species
Anti-mouse IgG -Peroxidase antibody	1:10000	A9044, Sigma Aldrich	Rabbit
Anti-rabbit IgG -Peroxidase antibody	1:40000	A9169, Sigma Aldrich	Goat
Anti-goat IgG horse-radish conjugated	1:10000	2354, Santa Cruz	Mouse

Secondary antibodies were incubated for 1 h at room temperature whilst shaking.

Table 9: Fluorophore-coupled biomolecules

Fluorophore-coupled biomolecules	Dilution	Company
wheat germ agglutinin (WGA), Alexa Fluor 488 conjugate	5 µg/ml	Thermo Fisher Scientific
Hoechst	1:1000	H3570, Invitrogen

WGA-Alexa Fluor 488 was prepared in PBS and incubated for 1 h at room temperature in the dark.

Table 10: Antibodies for flow cytometry analysis

Antibodies	Dilution	Company	Species
Primary Antibodies against			
α-Smooth muscle-actin	1:1000	A2547, Sigma Aldrich	Mouse
IgG1	1:100	MAB002, R&D Systems	-
Secondary antibodies against			
Anti-mouse Alexa488	1:1000	A-11001, Invitrogen	Goat

Antibodies were prepared in blocking buffer and incubated for 45 min at 4°C.

2.7 Software

Table 11: Software

Analyses	Software
Flow cytometry analysis	flowingsoftware.btk.fi, Perttu Terho
Image processing and analyses	ImageJ
Immunoblot	ImageLab 5.1
Immunofluorescence	Xcellence pro (Olympus)
Multi-mode microplate reader measurements	SoftMax Pro 5.4
Proliferation assay	Cellavista
Rheological measurements	TRIOS (TA Instruments)
Statistical analysis	Microsoft Excel, GraphPad Prism 6

2.8 Cell biology methods

2.8.1 Thawing and culturing of normal human cardiac fibroblasts (hCF)

hCF were thawed in a 37°C water bath, the content of the cryovial was transferred to a tube, and the cryovial was washed with 1 ml FGM-3 containing supplements, FCS-50 and 1% Pen/Strep. Cells were cultured at 37°C and 5% CO_2 in T75 culture flasks. The medium was changed the next day to remove residual DMSO and afterwards every second day.

2.8.2 Thawing and culturing of tsA201 cells

TsA201 cells were thawed in a 37°C water bath and afterwards cultured in an appropriate medium containing DMEM (1x) + GlutaMAX supplemented with 10% heat-inactivated FBS and 1% PenStrep. The medium was changed every three to four days. Cells were cultured at 37°C and 5% CO_2.

2.8.3 Thawing and culturing of HyPer-expressing tsA201 cells

TsA201 cells expressing the genetically encoded sensor for H_2O_2, HyPer, were thawed in a 37°C water bath and afterwards grown in a culture medium containing DMEM (1x) + GlutaMAX supplemented with 10% heat- inactivated FBS and 1% PenStrep. Five µg/ml Puromycin was added to the medium to select the HyPer-expressing cells as they are additionally provided with a gene conferring resistance against Puromycin. Cells were cultured at 37°C and 5% CO_2, the medium was removed every three days.

2.8.4 Passaging and freezing of cell lines

To provide a preferably high viability and proliferation rate, cells were passaged after reaching a confluency of 80 – 95% by aspirating the old medium and washing the cell layer once with DPBS. Afterwards, they were incubated with 5 ml pre-warmed TripleE dissociation reagent per T75 culture flask for 3 min at 37°C. The detachment was visually evaluated under the light microscope. The enzymatic reaction was stopped by adding the same volume of growth medium. Cells were resuspended, cell number and viability were assessed by electrical current exclusion, using the CASY TTS. A fraction of the cell suspension was seeded in the required density into a fresh medium containing culture vessel.

To create stock aliquots of the cell lines the obtained cell suspension was centrifuged for 10 min at 100 x g and 4°C to pellet the cell suspension, the supernatant was removed, and the cells were resuspended in freezing medium (10% DMSO in FBS). Cryovials containing 2-4x10^6 cells/ml

were transferred to a freezing container, filled with isopropanol, which allowed for gradually freezing at – 80°C. The other day the cryovials were transferred to – 152°C for long-term storage.

2.8.5 Proliferation assay

hCF were seeded as described in 3.1.1 at a density of 25000 cells/well in a 24-well plate. In addition, tsA201 cells were seeded at a density of 25000/well in a 24-well plate to assess possible cell-line specific effects. Cells were treated with different concentrations of pirfenidone (0, 0.1, 0.3, 1.0 or 3.0 mg/ml dissolved in FGM-3 or tsA201 growth medium, respectively). hCF were fixed on day 0 (after 24 h), 2, and 4, whereas tsA201 cells were fixed on day 0, 2, and 3, due to their higher proliferation rate. Medium and treatment were changed every second day. To fix the cells, the medium was removed, and each well was washed with 500 µl PBS. Afterwards, the cells were incubated with 300 µl of 4% PFA in DPBS for 10 min. PFA was removed and the cell layer was covered with 1 ml PBS to prevent from drying-out. The plates were kept in the fridge at 4°C until measurement.

For nuclear staining 4', 6-diamidino-2-phenylindole (DAPI) was used. Therefore, the PBS was removed from the wells and replaced with 400 µl of 0.1% DAPI in PBS. The plates were incubated at 4°C on a shaker for 30 min in the dark, followed by washing with PBS. Automated evaluation of the cell number was assessed either by automated counting using the Cellavista System (hCF) or by measuring the relative immunofluorescence units with the FlexStation 3 multi-mode microplate reader (tsA201).

2.8.6 Toxicity assay

hCF were seeded at a density of 50000/well in a 24-well plate and cultured until they reached a confluency of 90%. The cells were treated with 0, 0.1, 0.3, 1 and 3 mg/ml pirfenidone in FGM-3 for 48 h. For live staining, the medium was removed and the plates were incubated with Hoechst33342 (10 µg/ml) and propidium iodide (0.5 µg/ml) in PBS for 30 min. Cell number and death were analyzed with the help of the Cellavista System.

2.8.7 Generation of engineered connective tissue from NHCF (ECT)

hCF were cultured as described in 3.1.1. The collected cells were counted using the CASY TT system (Roche), and subsequently centrifuged at 100 x g and 4C° for 4 min. All required materials were pre-chilled and all following steps were performed on ice. The cells were

resuspended in the correct amount of supplemented fibroblast growth medium, according to the number of required ECT. The ECT master mix was prepared by pipetting bovine collagen type I, DMEM 2x, and NaOH into a 50 ml tube, according to table 12. At last, the cell suspension was added and mixed carefully. ECT were cast into either flexible moulds in a 48-well plate or stiff moulds by adding 180 µl in circular motion into the wells.

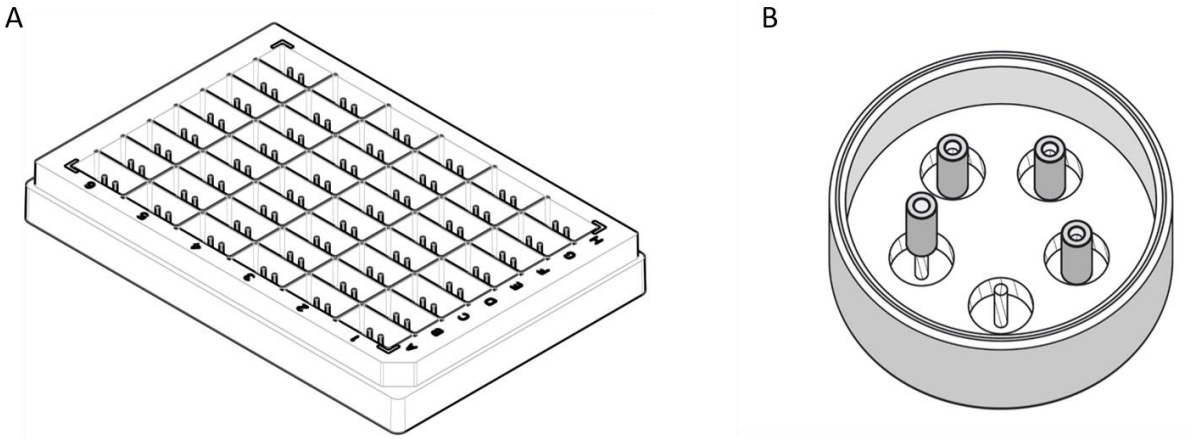

Figure 6: Technical schemes of casting moulds. (A) The plate with 48 moulds, equipped with flexible poles is shown. ®Myriamed GmbH**(B)** Self-made circular casting moulds with stiff poles are shown.

The ECT were kept in the humidified incubator at 37°C for 1 h to condensate. Afterwards, 0.5 ml per well of supplement fibroblast growth medium without treatment or with 0.3 or 1.0 mg/ml pirfenidone was added. The ECT were treated for 5 days. The medium was changed every second day including the additives.

Table 12: Composition of the ECT master mix per tissue

Master mix component	**Volume (µl)**
Collagen: 0.3 mg/ECT (stock: 6.49 mg/ml)	46.3
2x DMEM (supplemented)	46.3
0.1 M NaOH	3
Total cell number: 0.75 x 10^6/ECT (suspension: 9.056 x 10^6/ml)	84.4
Total volume	180
Number of ECT	1

For one ECT, 180 µl plus 10% safety volume of the ECT master mix must be prepared. Hence, for 30 ECT a total volume of 5.94 ml is needed.

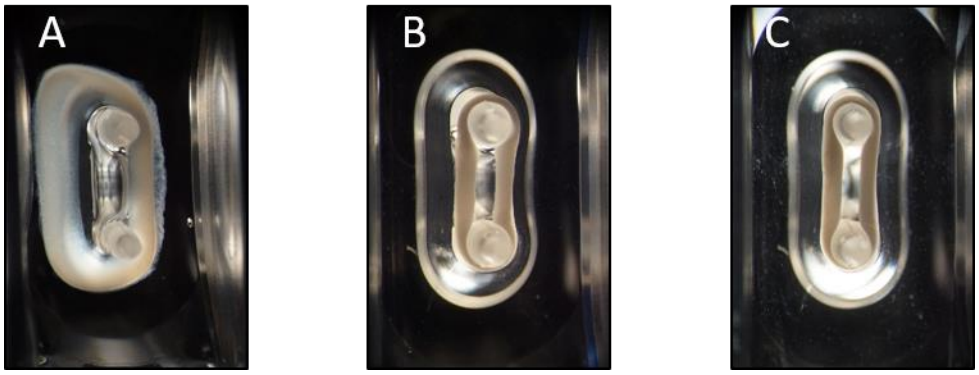

Figure 7: Representative images of a control ECT in a flexible mould at different culture days. (A) The image shows an ECT 1 h after casting. **(B, C)** Images of ECT on Day 2 and 5 are shown.

The fluorescence of the UV-excitable poles of the flexible ECT in the 48-well plates was measured every day to visualize the deflection of the poles. The plate was imaged under UV_A-light to make the UV-dye containing poles visible. Afterwards, the distance between the poles was analyzed using ImageJ and relative changes compared to day 0 were calculated.
Both, flexible and stiff ECT were imaged every day to compare occurring differences in tissue shape and size.

2.8.8 Destructive tensile strength measurements

On day five, engineered tissues were imaged using a stereomicroscope Lumar.V12 (Zeiss) from top and side to measure the cross-sectional area (CSA). The analysis is described in 3.5.1.
To assess the biomechanical properties of the tissues, destructive tensile strength measurements were performed using a RSA-G2 dynamic mechanical analyzer (TA instruments). Therefore, the ECT were fixed between two hooks in an organ bath filled with DPBS tempered to 37°C. Before starting the measurement, the force and the gap were set to zero. The tissues were then stretched with a constant linear rate of 0.03 mm/s until the point of rupture. The analysis is described in 3.5.1.

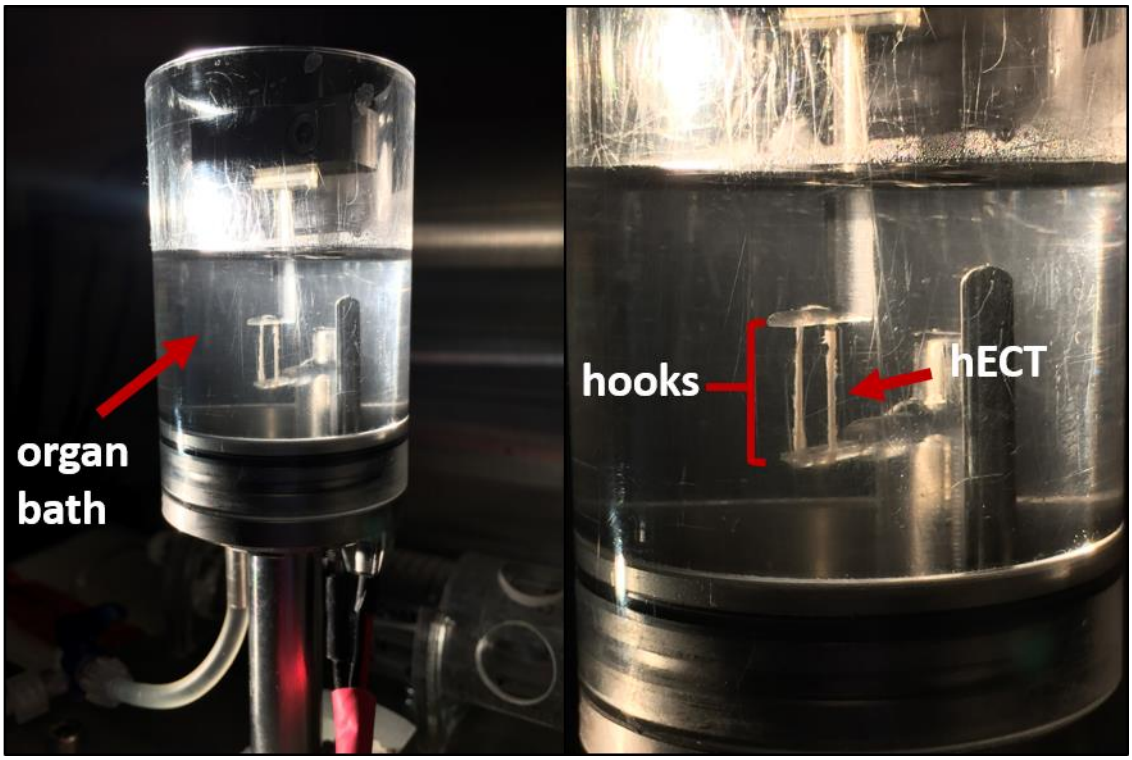

Figure 8: Destructive tensile strength measurements. The ECT is fixed between two custom-made hooks in a tempered organ bath and stretched at a linear rate until rupture.

Depending on further experiments ruptured or non-ruptured ECT were snap-frozen in 2 ml microtubes using liquid nitrogen and stored at -80°C.

2.8.9 Isolation of cells from ECT

ECT were dissociated by transferring each tissue into a well of a 24-well plate containing 1 ml pre-warmed collagenase solution (2 mg/ml collagenase I and 20% FBS in calcium-containing PBS). The tissues were incubated for 1-3 h at 37°C. The supernatant was transferred into pre-chilled 15 ml tubes. The tissues were washed once with 1 ml pre-warmed DPBS (w/o calcium). After washing, the DPBS was collected into the pre-chilled tube and each ECT was incubated with 1 ml pre-warmed dissociation solution, containing Accutase, 0.025% trypsin and 20 µg/ml DNAse, at 37°C for 30 min. The remaining tissue fragments were pipetted several times and subsequently 1 ml DPBS containing 5% FBS was added to each well. The cell suspension was transferred into the collection tube and each well was washed again with 1 ml DPBS containing 5% FBS to make sure that preferably all cells from the well were collected. The collection tube was kept on ice during all steps. The suspension was centrifuged at 100 x g for 10 min at 4°C. The supernatant was discarded and the pellet resuspended in 1-2 ml ice-cold DPBS + 5% FBS. The cell number was assessed by using the CASY TT (Roche). The cell suspension was again

centrifuged at 100 g for 10 min at 4°C. The supernatant was discarded and the pellet resuspended in 2 ml of ice-cold 4% PFA, which was added dropwise while the falcon was held onto the vortex. After incubating for 5 min on ice, the cell suspension was again centrifuged at 100 g for 10 min at 4°C, the supernatant was discarded, and the pellet was resuspended in 1-2 ml ice cold DPBS. The fixed samples were stored at 4°C for up to 1-2 weeks.

2.9 Intracellular H_2O_2 measurement

To monitor the redox-level of HyPer in tsA201 cells, the cells were seeded into 96-well imaging plates at a density of 20.000 cells/well and kept under normal growth conditions, as previously mentioned, until reaching a confluent state. The cells were treated with 0 or 1 mg/ml pirfenidone for 4 h. Serial dilutions (0, 10, 100 and 1000 μM) of H_2O_2 with FRET buffer were prepared and 200 μl per well was added to an unsterile 96-well compound plate. After incubation, the cells were washed twice with 100-200 μl PBS and 180 μl of pre-warmed FRET buffer was added to each well. The measurements were performed using the FlexStation 3 multi-mode microplate reader at 37°C. HyPer was excited at 405 and 488 nm and the fluorescence emission at 520 nm. After 60 s, 20 μl of H_2O_2 from the compound plate was added to the cells. The measurements were carried out for 300 s in total.

2.10 Histological methods

2.10.1 Fluorescence staining of the actin cytoskeleton, the nucleus, and the membrane system

DAPI staining was used to visualize nuclear changes, like fragmented bodies and condensed or deformed nuclei, which occur in apoptotic or necrotic cells (Atale et al. 2014). Additionally, WGA was chosen as it is a common dye to picture secretory membrane systems, including the Golgi complex and the plasma membrane, due to its interactions with sialic acid and N-acetylglucosamine residues in glycoproteins or glycolipids (Chazotte 2011). Ultimately, TRITC-phalloidin was used to stain filamentous actin (f-actin), in order to evaluate the level of stress fibre formation (Cano et al. 1992).

The fixed cells, after 2 days of treatment with pirfenidone (see section 3.1.5 Proliferation assay), were permeabilized with 0.2% Triton X-100 in PBS for 3-4 min. The cells were washed with PBS and stained with TRITC phalloidin (0.5 μg/ml), DAPI (1 μg/ml) and WGA- Alexa Fluor 488 (5 μg/ml). The staining was performed for 1 h at room temperature in the dark. Afterwards, the cells were washed with DPBS twice, and kept at 4°C in the dark until used for imaging. The

cells were imaged using an inverted fluorescence microscope (Olympus) at a magnification of 20x.

2.10.2 Cell cycle analysis performed by FACS

Cells isolated from the ECT (see section 3.1.9 Isolation of cells from ECT) were analyzed by using flow cytometry to quantify the ratio of the cells in different phases of the cell cycle. Therefore, the cell suspension was centrifuged at 300 x g for 5 min at 4°C and the supernatant was discarded. The pellet was resuspended in 200 µl blocking buffer, transferred into a 96-well round bottom plate, and permeabilized for 5 min at 4°C. After centrifuging at 300 x g for 5 min at 4°C and draining by inversion. Hoechst33342 in 50 µl/well blocking buffer was added (table 9) and incubated for 30 min on ice in the dark. Then, 150 µl PBS was added to each well. After centrifugation, the cellswere washed with blocking buffer, again resuspended in 200 µl PBS, and let pass through a strainer (70 µm) into a FACS tube to proceed with flow cytometry analysis. Using a LSRII SORP Cytometer (BD Biosciences), a hierarchical gating strategy was applied. Initially, the forward scatter area (FSC-A) versus sideward scatter area (SSC-A) was used as the first gate. Afterwards, cell debris was excluded by gating the DNA signal area versus FSC-A. To avoid doublet cells, the DNA signal width versus FSC-A was used as the following gate. Using the Flowing software (flowingsoftware.btk.fi, Perttu Terho) and this gating strategy, cycle phases (450/50 nm) were analysed and cells in G0/G1, S and G2/M phase were identified. There were at least 10.000 events per sample at a flowing rate beneath 100 events per second.

2.11 Protein biochemical methods

2.11.1 Isolation of protein from 2D-cultured cells

To prepare samples for protein analysis, the cells were seeded onto 6-well plates at a density of 150.000 cells/well. After reaching a confluency of 80-90%, the cells were treated with 0, 0.3, or 1.0 mg/ml pirfenidone for 4 h in duplicates. Subsequently, one of the duplicates was incubated with 5 ng/ml TGF-beta for 30 min. Afterwards, the medium was removed and the cells were washed with DPBS. The plates were kept on ice and 250 µl of ice-cold Cytobuster lysis buffer supplemented with protease and phosphatase inhibitor was added to each well. The cells were collected using a cell scraper and pipetted into a 1.5 ml reaction tube. The cell suspension was then centrifuged for 30 min at 12.000 x g and 4°C. The supernatant was transferred to a new reaction tube and snap-frozen using liquid nitrogen. The samples were stored at -80°C until required for further analysis.

2.11.2 Sodium dodecyl sulphate polyacrylamide gel electrophoresis (SDS-PAGE)

Sodium dodecyl sulphate-polyacrylamide gel electrophoresis (SDS-PAGE) was used for the separation of protein mixtures according to their molecular weight. To assure sufficient separation, a 5% stacking gel and resolving gels with different concentrations of acrylamide/bisacrylamide (6% or 12%, depending on the size of the proteins to be detected) were used.

Table 13: Components of stacking and resolving gel

Reagent	**Stacking gel 5%**	**Resolving gel**	
		6%	12%
ddH_2O	2.8 ml	2.6 ml	1.6 ml
1.0 M Tris/HCl, pH 6.8	0.38 ml	-	-
1.5 M Tris/HCl, pH 8.8	-	1.3 ml	1.3 ml
Acrylamide/bisacrylamide mix	1.3 ml	1.0 ml	2.0 ml
10% SDS	0.03 ml	0.05 ml	0.05 ml
10% APS	0.03 ml	0.05 ml	0.05 ml
TEMED	0.003 ml	0.004 ml	0.002 ml
Total volume	3 ml	5 ml	5 ml

The cell lysates were mixed with 4x SDS-PAGE loading buffer and incubated for 5 min at 95°C. The gel was loaded with 15 – 40 µl of the samples per lane, depending on the expression level of the protein. Electrophoresis was carried out at 190 V in 1x SDS running buffer for 1 h until the dye front ran out of the gel. Roti-Mark Standard and Roti Mark TRICOLOR protein ladder were used for protein size determination.

2.11.3 Immunoblotting

Following the SDS-PAGE, the separated proteins were electro-transferred onto a nitrocellulose membrane, using a transfer stack containing sponges, filter papers, the membrane and the gel. The stack was assembled in the transfer buffer and electrophoresis was carried out in ice-cold transfer buffer for 50 min at 100 V. The whole setup was additionally cooled with an icepack in the chamber. The successful transfer was verified by Ponceau-S staining. Therefore, the membranes were incubated in the staining solution for 3-5 min and the excessive dye was removed with distilled H_2O. Images of the stained membranes were taken and the membrane was cut into strips, according to the molecular weight of the specific proteins. After that, the

membranes were washed several times with TBS-T buffer until the staining was completely vanished. The membranes were blocked using the 1x Roti-Block for 1 h at room temperature. Subsequently, the membranes were incubated overnight with the specific primary antibodies in TBST-T (see table 7) at 4°C on a shaker. The membranes were washed three times with TBST-T, each for 10 min, and then incubated with the secondary antibodies in TBST-T (see table 8) for 1 h at room temperature. After that, the membranes were again washed thrice for 10 min, each with TBS-T. The protein signal was visualized using a chemiluminescence reagent in a ChemiDoc imaging system. The quantitative analysis was performed by using ImageLab 5.1 analysis software. For detection of the phosphorylation status of a certain protein, the membranes were incubated with Roti-Free Stripping Puffer 2.2 plus for 1 h at room temperature. Afterwards, they were washed with TBST-T and blocked by using the 1x Roti-Block for 1 h at room temperature. Subsequently, the membranes were incubated with another primary antibody and the same steps as described above were carried out.

2.12 Quantitative and statistical analysis

2.12.1 Stress strain analysis

By using the macroscopic pictures of the ECT tissues, the diameters were measured at minimum four different positions in both imaging planes. The CSA was calculated assuming an elliptical shape: $CSA = d/2_{mean\ top\ view} \times d/2_{mean\ side\ view} \times \pi$.

Data from the destructive tensile strength measurements were processed in Excel and the measured forces were divided by the CSA to obtain stress values (kPa). Afterwards, these values were plotted against the strain values calculated by the equation $(L_{total}-L_0)/L_0$ in which L_0 represents the initial gap between the upper and lower hook and L_{total} is the total gap at each point. To determine the Young's modulus, the slope of the linear region of the stress-strain-curve was determined by linear regression. Further important properties of the curves, like yield point strain (end of elastic region), maximum stress (highest stress point), and ultimate strain (sudden drop in stress) were identified manually. The toughness was calculated with the area under the curve function of Graphpad Prism7.

2.12.2 Statistical analysis

Experimental data are presented as means±SEM. Data was analysed by 1- or 2- way ANOVA. Statistical calculations were carried out by using GraphPad Prism 6/7. Significance was assumed when $p < 0.05$.

3. Results

3.1 Effects of pirfenidone on 2D-cultured cardiac fibroblasts

3.1.1 Pirfenidone treatment decreases the proliferation rate of hCF and tsA201 cells

Since there are only few data about pirfenidone and its effects on human cardiac fibroblasts, the first step was to perform a proliferation assay to determine an appropriate concentration for further experiments. According to previous studies (Lin et al. 2009; Shi Q et al. 2011) concentrations of 0.1, 0.3, 1.0, and 3.0 mg/ml were used. The treatment was carried out for 0, 2, and 4 days. Afterwards, the cells were stained with DAPI and cell number was assessed by automated counting using the Cellavista System.

As shown in figure 9, under control condition the cell number increased 5.5-fold within 4 days. In the presence of 0.1 and 0.3 mg/ml pirfenidone the cell numbers declined at day 5 compared to control by 20% and 32%, respectively. In the presence of 1 mg/ml no increase in cell number was observed compared to day 0 and the application of 3 mg/ml induced a complete loss of cells indicating that this concentration induces cell death.

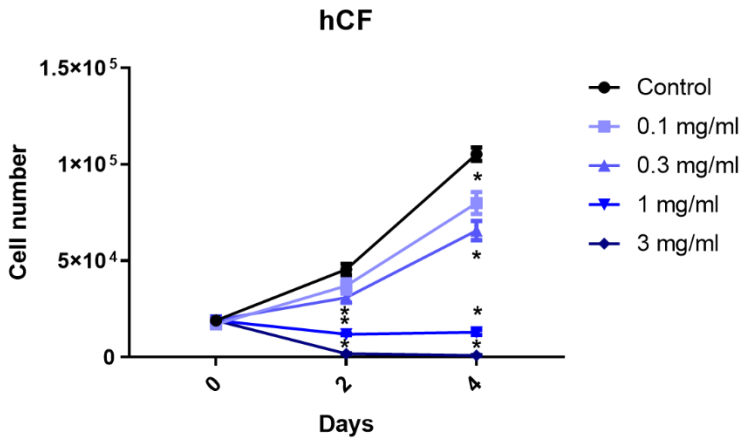

Figure 9: Proliferation assay of pirfenidone-treated hCF. 2D-cultured hCF were treated with different concentrations of pirfenidone (0, 0.1, 0.3, 1.0, 3.0 mg/ml) for 0, 2, or 4 days. The cell number was assessed by staining with DAPI and automatic counting. All values are means±SEM, n=3 – 4 in 4 replicates. Statistical analysis was performed by a 2-way ANOVA with a Dunnett's multiple comparison test vs. control, *p > 0.05.

To evaluate, if the observed effects were due to a cell-specific action of pirfenidone, a similar proliferation assay was performed with human embryonic kidney cells (tsA201 cells). The treatment was carried out for 0, 2, or 3 days. In contrast to the hCF, the tsA201 cells were not affected by the two lowest pirfenidone concentrations. However, a decreased proliferation rate

and milder cytotoxic effects were observed, when the cells were exposed to concentrations above 1.0 mg/ml (Fig.10).

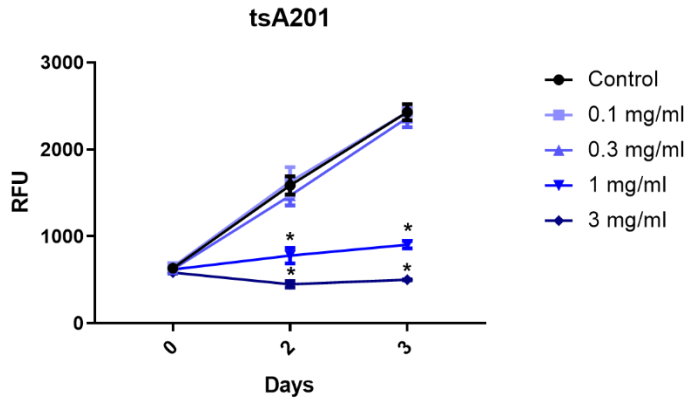

Figure 10: Proliferation assay of pirfenidone-treated tsA201 cells. 2D-cultured tsA201 cells were treated with different concentrations of pirfenidone (0, 0.1, 0.3, 1.0, 3.0 mg/ml) for 0, 2, or 3 days. The cell number was assessed by staining with DAPI and measuring the relative fluorescence units. All values are means±SEM, n=3 – 4 in 3 replicates. Statistical analysis was performed by a 2-way ANOVA with a Dunnett's multiple comparison test vs. control, *p > 0.05.

The differential effect of pirfenidone in both cell types was also reflected by the different calculated IC_{50} values, which were 0.43 mg/ml for hCF and 0.71 mg/ml for tsA201 cells (Fig.11).

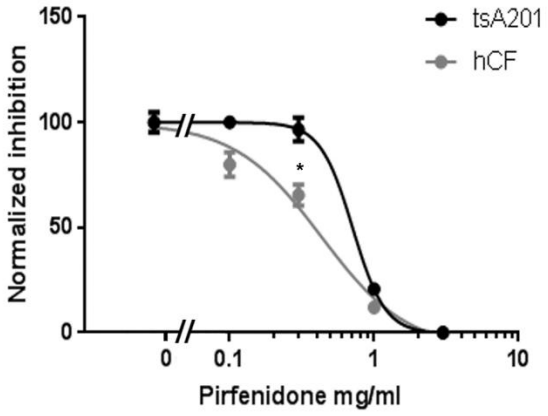

Figure 11: Comparison of the inhibitory effect of pirfenidone. A normalized comparison of the pirfenidone effect in two different cell lines is given. The IC_{50} values of pirfenidone on the decline in cell number were calculated by non-linear regression for day 5. (hCF IC_{50} = 0.43 mg/ml, tsA201 IC_{50} = 0.71 mg/ml). Shown are the means±SEM, n=3 – 4. The comparison was performed by a 2-way ANOVA with a Sidak's multiple comparison test, *p > 0.05.

Due to the observed cytotoxic effects of 3 mg/ml pirfenidone, this concentration was omitted in all further studies.

3.1.2 Cytotoxic effects of pirfenidone are dependent on hCF confluency

For further assessment of the observed cytotoxic effects, confluent hCF were treated with different concentrations (0, 0.1, 0.3 and 1.0 mg/ml) of pirfenidone for 48 h. To distinguish between viable and dead cell populations, a combined live staining of Hoechst33342 and propidium iodide was performed, as both dyes are staining DNA, but propidium iodide is only permeant to dead cells with a disrupted membrane (Atale et al. 2014).

Interestingly, no cytotoxic effects were observed at any concentration of pirfenidone (Fig.12). This indicates that the cytotoxic effect of pirfenidone is dependent on the confluency of hCF.

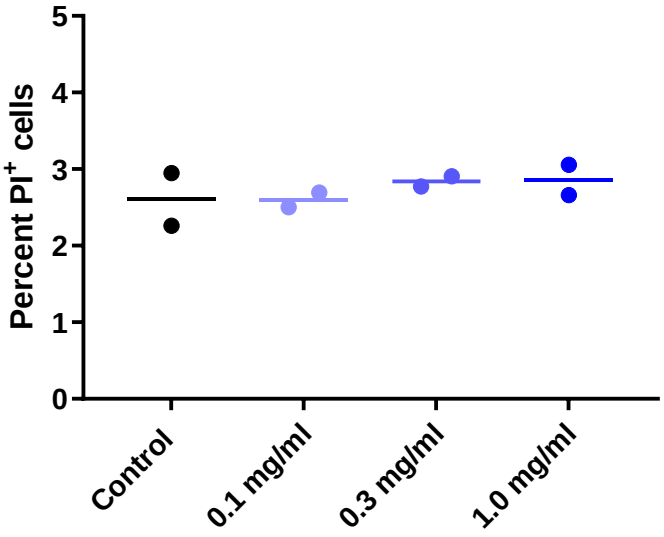

Figure 12: Assessment of cell number and cell death. Treatment of confluent hCF with 0, 0.1, 0.3, and 1.0 mg/ml pirfenidone for 48 h. Life staining was performed using Hoechst33342 and PI to analyse cell number and death. Given is the percentage of PI-positive cells of all cells detected with Hoechst33342. The values are given as means of 6 technical replicates from 2 independent experiments.

3.1.3 Pirfenidone shows no visible effects on actin stress fibre formation and glycosylation

Semi-confluent hCF were fixed after two days of pirfenidone treatment and stained with DAPI, WGA-Alexa Fluor 488, and TRITC-phalloidin to detect nuclei, glycosylation, and F-actin, respectively. The cells were imaged using an inverted fluorescence microscope (Olympus) at a magnification of 200x. Except the expected decrease in cell number, no striking differences in

actin fibre formation and glycosylation were observed. The nuclear and cell morphologies appeared to be unaltered (Fig. 13).

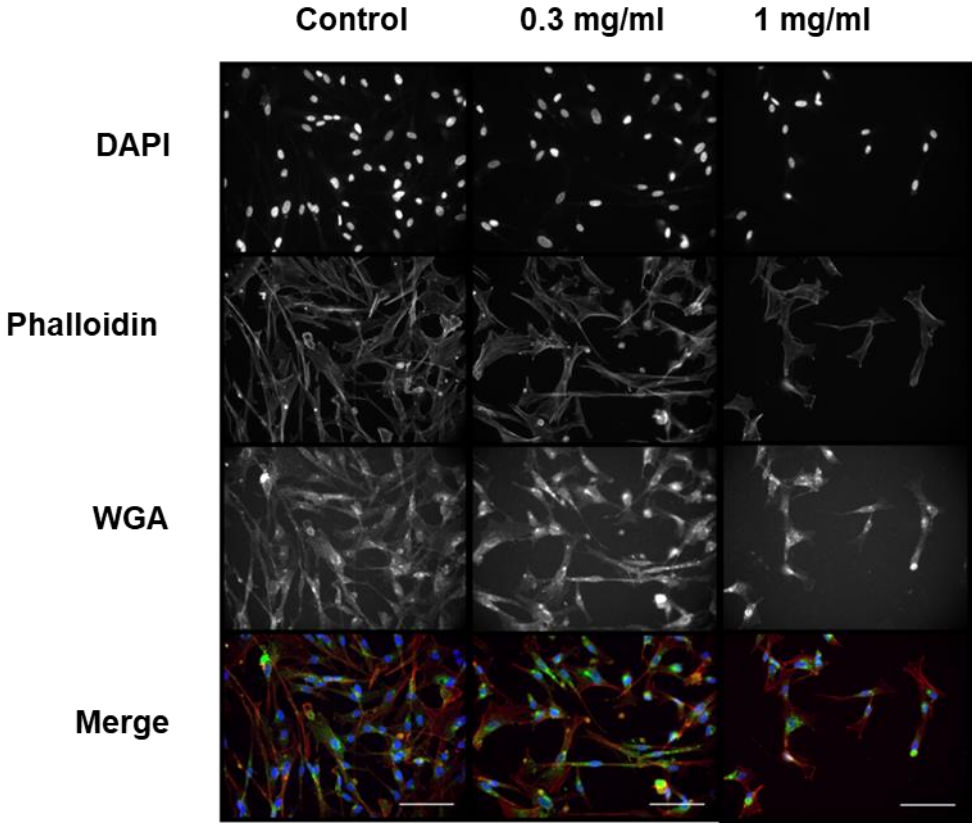

Figure 13: Fluorescence microscopy of 2D-cultured hCF after two days of pirfenidone treatment. hCF were treated with the indicated concentrations of pirfenidone for two days, fixed, stained, and imaged. Shown are representative images of different fluorescent stainings of the cell nuclei by DAPI (blue), F-actin by TRITC-phalloidin (red), and glycolipids and -proteins by WGA-Alexa fluor 488 (green). All images were taken with the same magnification (scale bar 100 μm). Merges, shown in the lower row, were generated with Xcellence pro software.

3.1.4 Pirfenidone affects canonical and non-canonical TGF-β signalling

Yet, no exact target of pirfenidone has been found, but many findings suggest that pirfenidone interacts with mediators of the TGF-β signalling pathway (Iyer et al. 1999; Hisatomi et al. 2012; Graziani et al. 2018; Park et al. 2019).

To assess if pirfenidone interferes with the canonical TGF-β signalling in hCF, confluent cell cultures of hCF were pre-incubated with different concentrations of pirfenidone (0, 0.3, and 1.0 mg/ml) for 4 h. Subsequently, 5 ng/ml TGF-β1 was added to one subset of the duplicates for 30 min. Afterwards, the cells were quickly lysed for protein phosphorylation analysis. As the

canonical signalling includes the direct phosphorylation of SMADs; SMAD2 and SMAD3 were the first proteins to be analysed.

The immunoblot analysis showed an expected increase of the phosphorylated SMAD2 and SMAD3 in the presence of TGF-β1. Additionally, the treatment with 0.3 and 1.0 mg/ml pirfenidone reduced the increase of SMAD2 phosphorylation in the presence of TGF-β1 by 27% and 42%, respectively. In contrast, SMAD3 phosphorylation was not significantly altered in the presence of TGF-β1, but slightly reduced under basal conditions (Fig. 14).

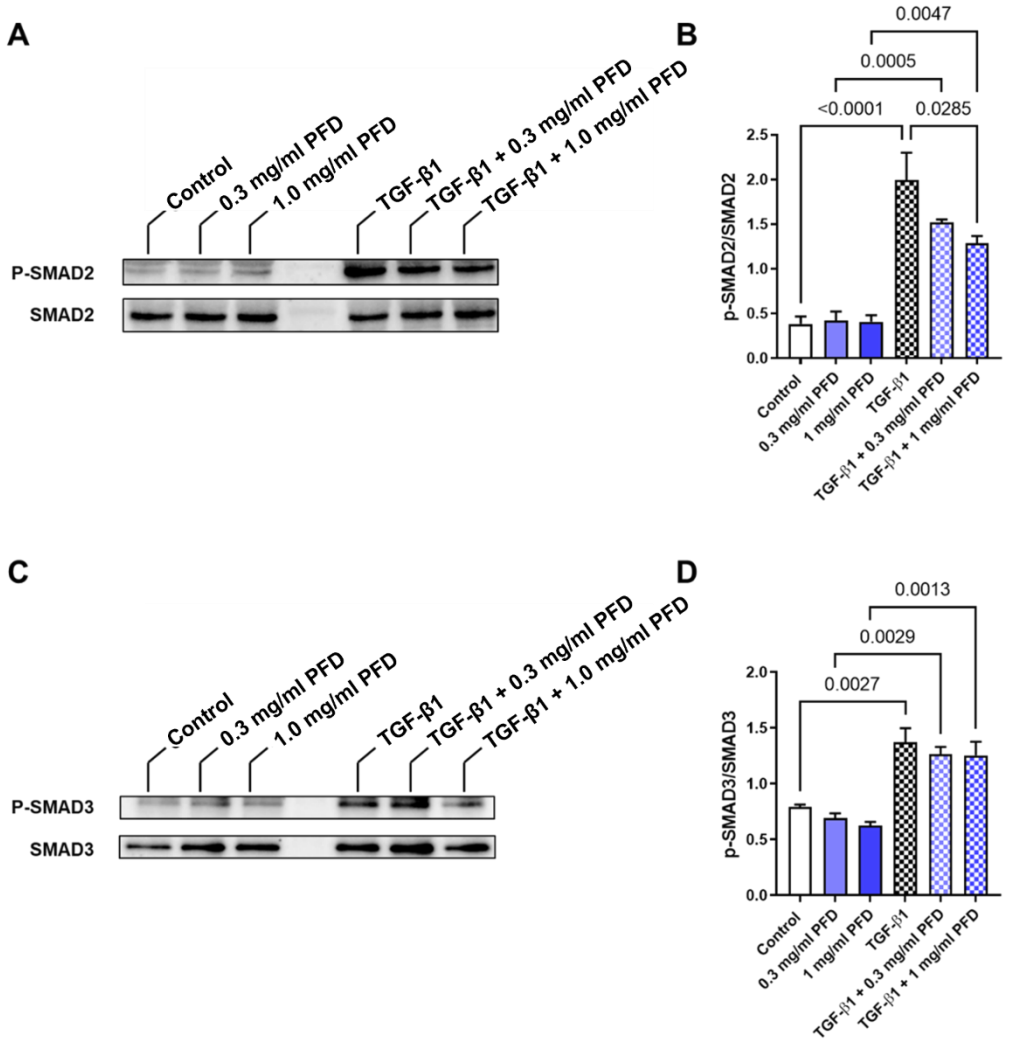

Figure 14: Immunoblot analysis of SMAD2 and SMAD3 phosphorylation. hCF were treated with 0.3 or 1.0 mg/ml pirfenidone (PFD) for 4 h and then 5 ng/ml TGF-β1 was applied for 30 min. Cell lysates were used for immunoblot analysis and representative immunoblots of total and phosphorylated SMAD2 **(A)** and SMAD3 **(C)** are shown. **(B, D)** In the bar graphs the changes in phosphorylated SMAD in relation to total SMAD expression is given of 3

independent experiments. Shown are means+SEM and p-values as assessed by 1way-ANOVA with Tukey's multiple comparison test.

Additionally, the non-canonical TGF-β1 signalling was studied by analysing the phosphorylation status of MAPK ERK1/2. The surprising results indicated that TGF-β1 did not increase ERK1/2 phosphorylation. The highest pirfenidone concentration, however, almost halved the amount of phosphorylated ERK1/2 under basal conditions and in the presence of TGF-β1 (Fig.15).

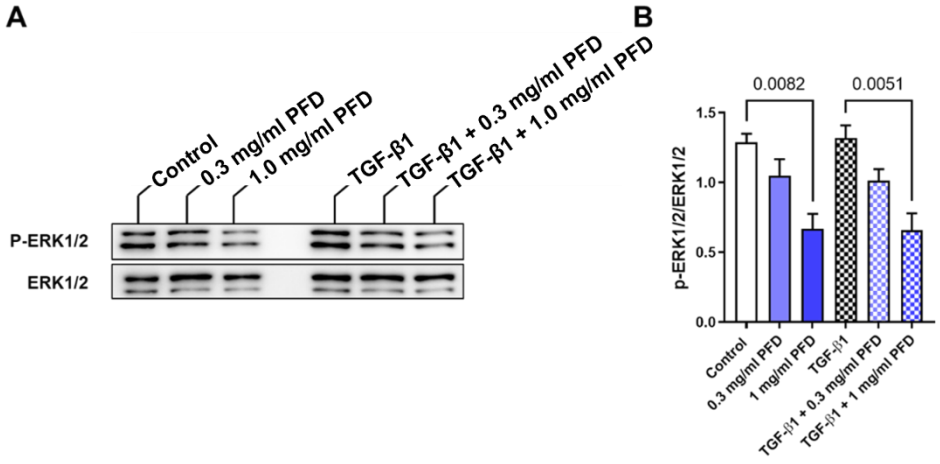

Figure 15: Immunoblot analysis of MAPK (ERK1/2) phosphorylation. hCF were treated with 0.3 or 1.0 mg/ml pirfenidone (PFD) for 4 h and then 5 ng/ml TGF-β1 was applied for 30 min. Cell lysates were used for immunoblot analysis. **(A)** Representative immunoblots of total and phosphorylated MAPK ERK1/2 are shown**. (B)** In the bar graphs the changes in phosphorylated ERK1/2 in relation to total ERK1/2 expression is given of 3 independent experiments. Shown are means+SEM and p-values as assessed by 1way-ANOVA with Tukey's multiple comparison test.

To evaluate if pirfenidone also influences kinases that are more up-stream in the signalling pathway of ERK1/2, the next proteins to be tested were MEK1/2.
Interestingly, effects similar to those of the ERK1/2 phosphorylation were observed, as the phosphorylation of MEK1/2 was not only reduced after TGF-β1 treatment, but also under non-stimulated conditions when treated with pirfenidone. The effects were even more pronounced as this time also the lower pirfenidone concentration led to a significant reduction of phosphorylated MEK1/2 in both conditions (Fig. 16).

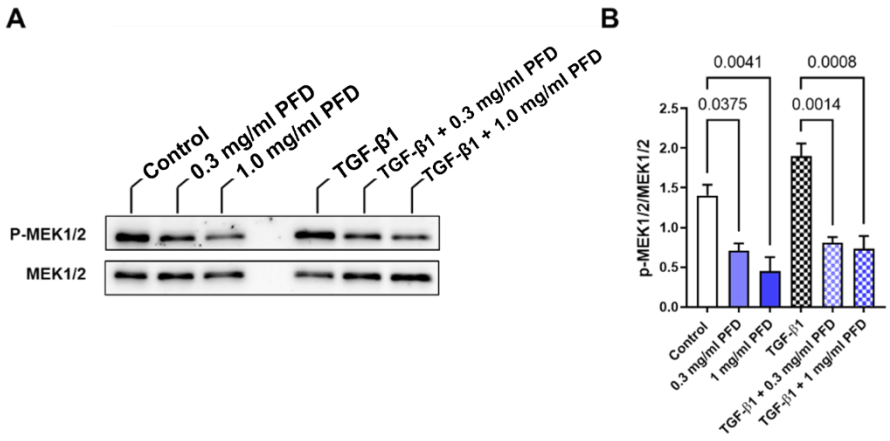

Figure 16: Immunoblot analysis of MEK1/2 phosphorylation. hCF were treated with 0.3 or 1.0 mg/ml pirfenidone (PFD) for 4 h and then 5 ng/ml TGF-β1 was applied for 30 min. Cell lysates were used for immunoblot analysis. **(A)** Representative immunoblots of total and phosphorylated MEK1/2 are shown**. (B)** In the bar graphs the changes in phosphorylated MEK1/2 in relation to total MEK1/2 expression is given of 3 independent experiments. Shown are means+SEM and p-values as assessed by 1way-ANOVA with Tukey's multiple comparison test.

3.1.5 Pirfenidone does not show reductive properties against H_2O_2 in tsA201 cells

Previous studies showed that pirfenidone owns anti-oxidative properties and can suppress the generation of intracellular ROS (Misra and Rabideau 2000; Monsalvo-Villegas et al. 2018; Ruwanpura et al. 2020). To study these effects, tsA201 cells expressing the redox sensor HyPer were treated with 0 or 1 mg/ml pirfenidone for 4 h. Different concentrations of H_2O_2 were added 60 seconds after the imaging measurements started. The ratio of the fluorescence intensity of the oxidized wavelength was divided by the fluorescence intensity of the reduced wavelength (I_{488}/I_{405}). That ratio was normalized to the average ratio of each well before the compound was added (0-60 seconds).

When the oxidative compound was added, the anticipated increase in the ratio was observed. Surprisingly, the reestablishment of the reductive cytoplasmic environment was significantly decelerated in the presence of pirfenidone compared to the control group. In both conditions, the higher H_2O_2 concentration did not alter the redox state as much as the lower concentration, indicating that there might be cytotoxic side effects with 1 mM H_2O_2 (Fig. 17).

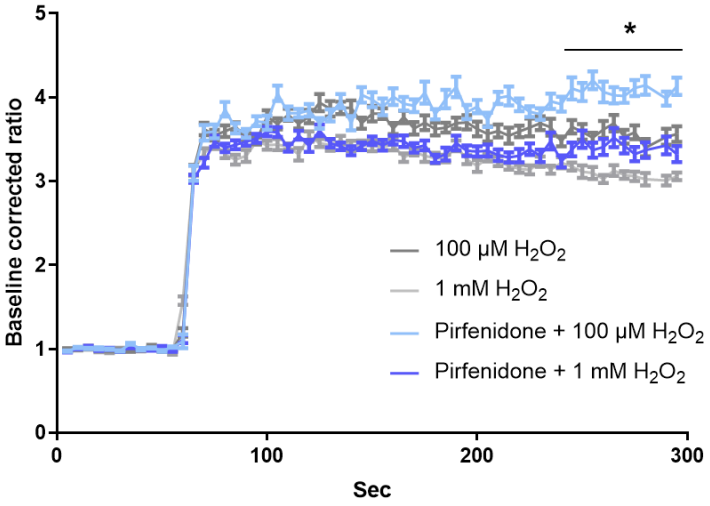

Figure 17: Changes of the intracellular redox level after application of H2O2. tsA201 cells, which stably expressed the redox sensor HyPer, were pre-incubated with 0 or 1 mg/ml pirfenidone and 100 µM or 1 mM H2O2 was added after 60 s basal reading. Shown is the baseline corrected ratio of the oxidized to reduced wavelengths normalized to the average ratio of each well before compound addition. Given are the means±SEM, n=5, *p<0.05 pirfenidone + 100 µM H_2O_2 vs. 100 µM H_2O_2 by 2way-ANOVA with a Tukey's multiple comparison test.

3.2 Effects of pirfenidone in ECT

3.2.1 Pirfenidone increases the cross-section area of ECT

To evaluate if pirfenidone influences the biomechanical properties of 3D-cultured hCF, ECT were generated by using hCF and bovine collagen I. The tissues were cultured in two different mould types. A casting model with two flexible poles was used to represent almost healthy-like tissue properties, whereas a second model with only one stiff pole was used to display a more stiff environment. After five days, the CSA were calculated by measuring the tissue diameters from top and side view imaging planes.

The macroscopic images of the ECT already indicated differences in tissue compaction after pirfenidone treatment. The treated tissues appeared to be more voluminous, compared to control tissues. In line, analysis of the measured diameters and subsequent calculation of the CSA revealed a significant increase in the CSA in both tissue models in response to pirfenidone compared to control. This increase was concentration-dependent (Fig. 18).

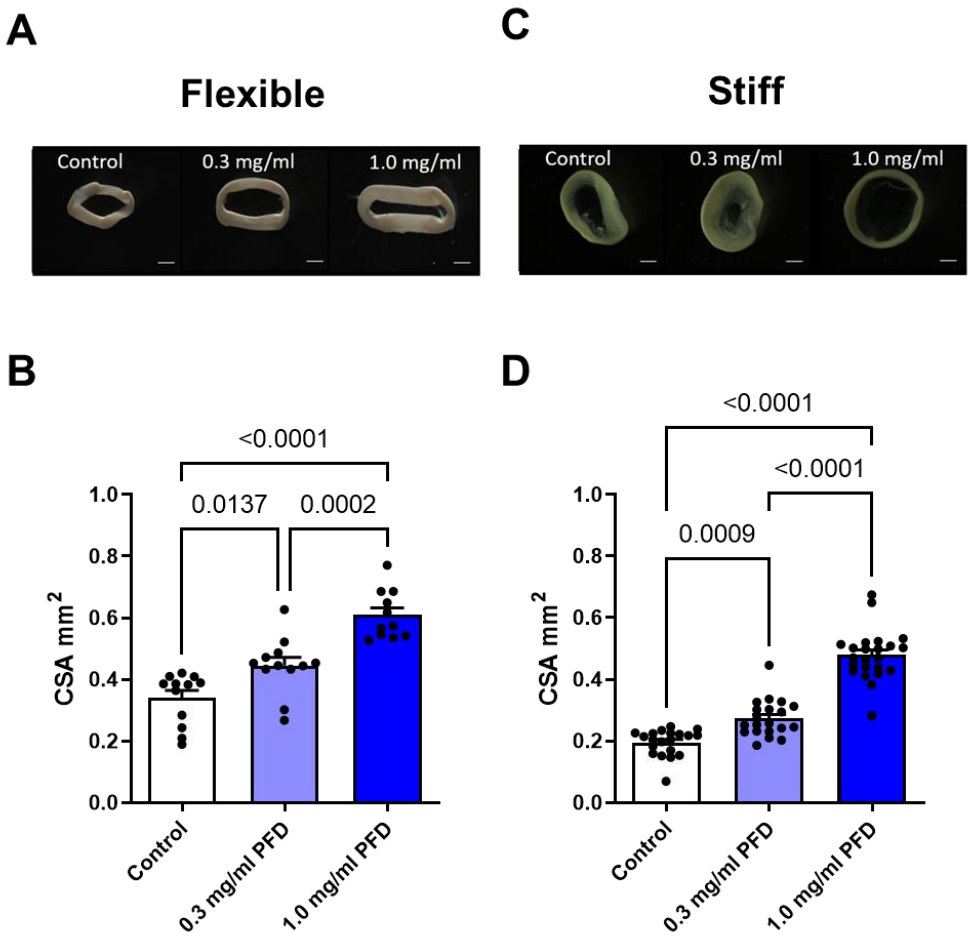

Figure 18: Morphological changes of the ECT and comparison of the CSA after pirfenidone treatment. ECT were generated with hCF and bovine collagen I. Representative images of ECT after culturing in flexible **(A)** or stiff **(B)** casting moulds and treatment with different concentrations of pirfenidone (0, 0.3, 1.0 mg/ml) for five days are given (scale bar = 1 mm). The bar graph summary of the calculated CSA of ECT cultured in flexible **(C)** or stiff casting moulds **(D)** is given, the values are means+SEM, flexible n=11-12, stiff n=20-23, p-values are given as assessed by 1way-ANOVA with Tukey's multiple comparison testing.

The contraction, which was evaluated by measuring the deflection of the poles of the flexible moulds, showed a distinct increase from day 0 to day 2 in the control as well as in treated tissues. Whereas the contraction of ECT without treatment and with the lower pirfenidone concentration still slowly increased until day 5, the contraction of ECT treated with 1.0 mg/ml pirfenidone reached a stable contraction niveau that was significantly lower compared to the other groups (Fig. 19).

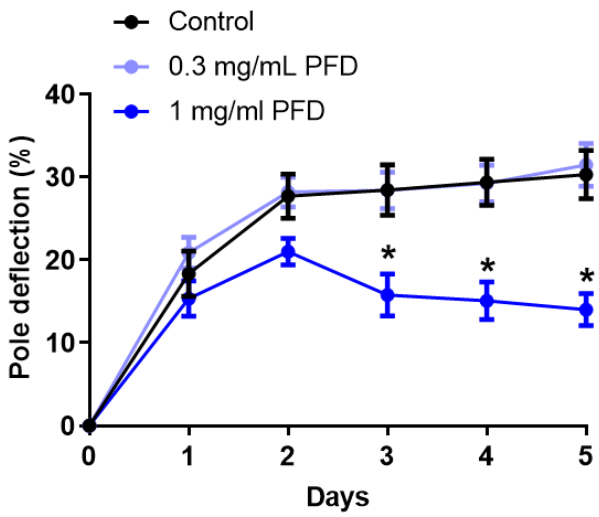

Figure 19: Effect of pirfenidone on pole deflection of flexible ECT. ECT were generated with hCF and bovine collagen I in flexible moulds and were cultured with different concentrations of pirfenidone (0, 0.3, 1.0 mg/ml, PFD) for five days. Pole deflection was detected every day and calculated in relation to day 0. All values are given as means±SEM, 18 ECT per group, *p < 0.05, *compared to control and to 0.3 mg/ml PFD, assessed by 2way-ANOVA with Tukey's multiple comparison test.

3.2.2 Pirfenidone influences the biomechanical tissue properties

On day five of culturing, destructive tensile strength measurements of the ECT were performed. Essential tissue properties, like the Young's modulus (stiffness), the yield point strain (elasticity), the maximum/ultimate stress (strength), and the ultimate strain at the failure point (extensibility) were determined (Fig.20).

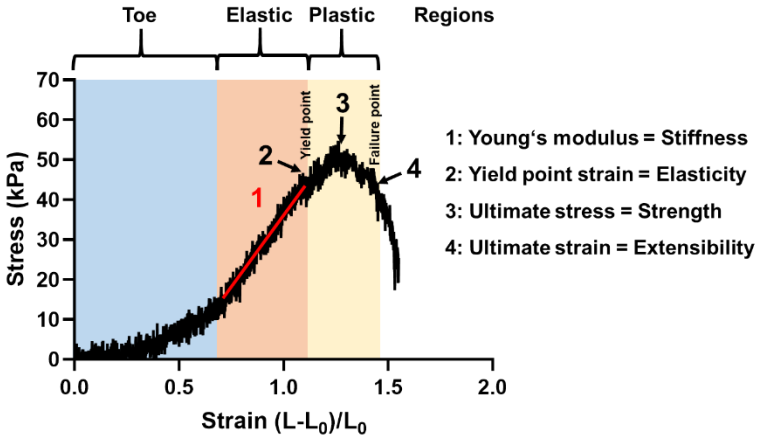

Figure 20: Representative stress-strain curve obtained by destructive tensile strength measurement of a representative ECT. Important parameters of the curve are highlighted.

An overall comparison of the two tissue models showed that under control condition ECT prepared in flexible moulds are less stiff and strong, but more elastic and extensible than ECT prepared in stiff moulds. For example, the Young' modulus of the flexible control ECT was around four times lower than the one of the stiff controls, whereas the ultimate strain was twice as high. Pirfenidone treatment showed only an effect in the highest concentration. It reduced the stiffness in the flexible and stiff model. And moreover, it reduced the ultimate stress and increased the yield and ultimate strain in the stiff model (Fig. 21).

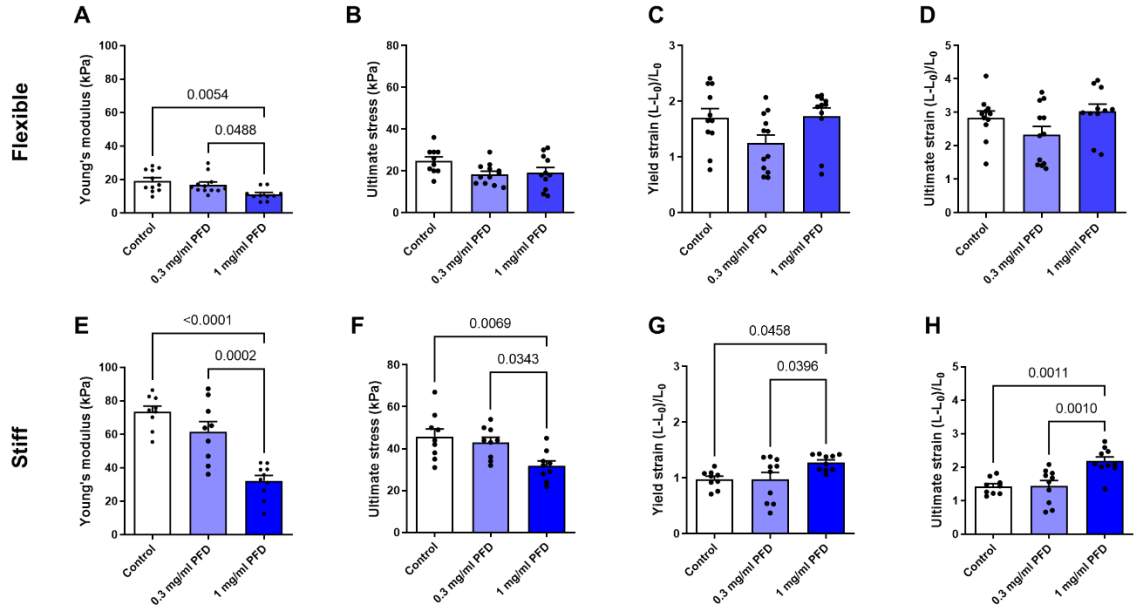

Figure 21: Analysis of biomechanical properties of control and pirfenidone-treated ECT. ECT were generated in flexible **(A-D)** or stiff **(E-H)** moulds and treated for 5 days with pirfenidone (PFD). Destructive tensile strength measurements were performed and the following parameters were retrieved from the stress-strain curves: Young's modulus (stiffness), ultimate stress (strength), yield strain (elasticity), and ultimate strain (extensibility). The bar graph summaries present the means+SEM, flexible n=10 – 12, stiff n=9 – 10, p-values were assessed by 1way-ANOVA with Tukey's multiple comparison test.

3.2.3 Higher pirfenidone concentrations affect cell viability

As inhibitory effects of pirfenidone on the proliferation rate were observed in 2D-cultured hCF, the cell number and viability of the ECT was additionally investigated. Therefore, the ECT were dissociated and the embedded cells were re-isolated and analysed by electrical current exclusion. In general, only a minor proportion of the initially added 750.000 cells could be re-isolated in both models. In the flexible model, around 200.000 cells could be reisolated and in the stiff model around 300.00 cells. Despite the higher number of reisolated cells in the stiff model, the

viability of these cells were also higher as in the flexible model. In both cases, 1 mg/ml pirfenidone showed a significant decline in total cell number as well as cell viability (Fig. 22).

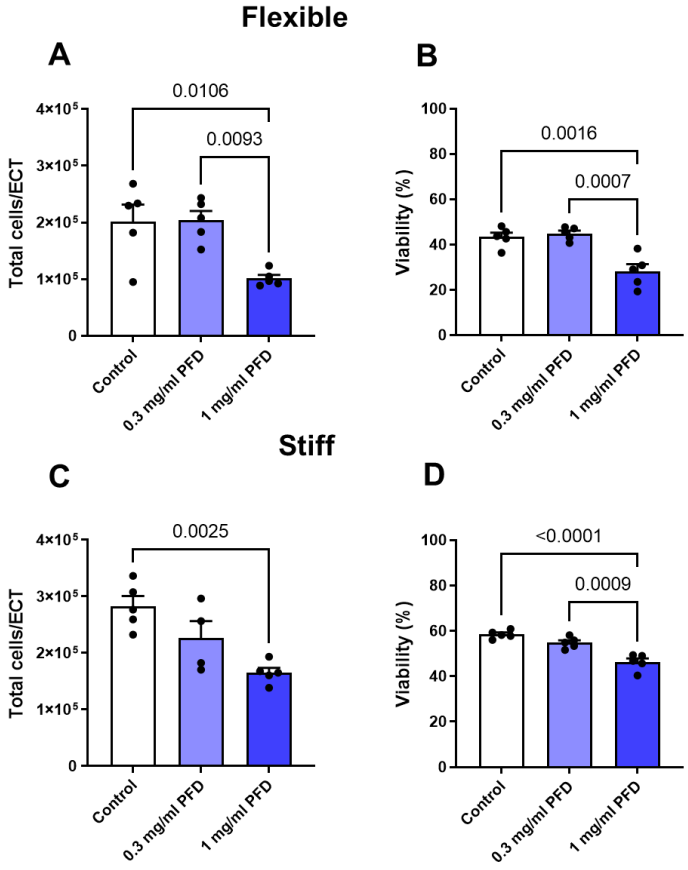

Figure 22: Pirfenidone reduces viability and cell number in a dose-dependent matter. ECT were generated in flexible **(A, B)** or stiff **(C, D)** moulds and treated for 5 days with pirfenidone (PFD). The hCF were isolated and the number of total isolated cells as well as the viability of the cells were analysed. The bar graph summaries display the means+SEM, flexible n=5, stiff n=4 – 5, p-values were assessed by 1way-ANOVA with Tukey's multiple comparison test.

3.2.4 Pirfenidone influences the ratio of cells in different phases of the cell cycle

For further assessment of the phenotype of the hCF, the re-isolated cells were analysed by flow cytometry and the percentages of cells in the different phases of the cell cycle were quantified. As depicted in Fig. 23, treatment with 1 mg/ml pirfenidone increased the portion of cells in G0/G1 phase of the cell cycle in both models, while it decreased the number of cells in S and G2/M-phase.

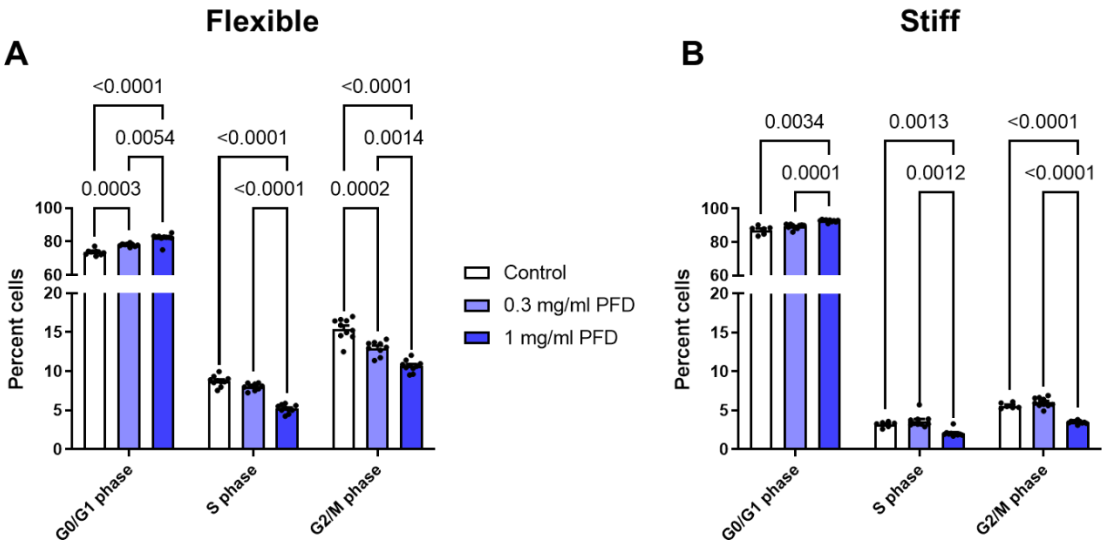

Figure 23: Flow cytometry analysis of the cell cycle of re-isolated hCF. ECT were generated in flexible **(A)** or stiff **(B)** moulds and treated for 5 days with pirfenidone (PFD). The hCF were isolated and a cell cycle analysis was performed. In the bar graph summaries the percentages of cells in each cell cycle phase are shown. Given are the means+SEM, flexible n=9 – 10, stiff n=6 – 10, p-values were assessed by 2way-ANOVA with Tukey's multiple comparison test.

4. Discussion

Cardiac fibrosis is still considered as one of the major problems in heart diseases. But despite the growing demand, no effective treatment is available to halt the pathological mechanisms that eventually lead to heart dysfunction or even organ failure.

The process of fibrotic remodelling does not only occur in cardiac tissue. Fibrosis of the lung, the intestines, the joints, or the skin (Lopez-de la Mora et al. 2015) represent urgent issues of the modern medicine. Multiple experiments applying different cell types and organs led to the conclusion, that similar molecular pathways are activated during the development of a fibrotic state. These findings led to the transfer of treatment strategies from one fibrotic disease to the other. One example is the small molecule pirfenidone, which has proven beneficial effects in the treatment of idiopathic pulmonary fibrosis by reducing the decline of forced vital capacity and the disease progression (Somogyi et al. 2019; Ruwanpura et al. 2020). These strong effects, combined with an adequate safety and no severe adverse reactions, make pirfenidone a promising new anti-fibrotic agent also for other fibrotic diseases, including cardiac fibrosis.

Many investigations were carried out approaching the anti-fibrotic properties of pirfenidone in different tissues. The results of *in vitro* studies showed similar outcomes, like inhibition of fibroblast proliferation, TGF-β-mediated differentiation into myofibroblasts, and ECM deposition (Iyer et al. 1999; Lin et al. 2009; Conte et al. 2014; Shah et al.). Importantly, many studies were performed with the help of 2D cultures, which are missing the complex 3D environment. However, fibrosis is highly connected to changes in the ECM, and therefore the biomechanical properties of the tissue, thus studies in 2D are not sufficient to evaluate the anti-fibrotic effects of a drug. Hence, in this study 2D experiments were combined with studies with engineered connective tissues generated from hCF to gain more insights in the capacity of pirfenidone to halt pro-fibrotic processes of activated cardiac fibroblasts.

4.1 Effects on the proliferation of hFC and tsA201 cells

The differentiation from quiescent hCF into activated myofibroblasts is one of the central pathways in the pathogenesis of cardiac fibrosis. In a first step of this process an enhanced proliferation of activated hCF was observed (Wynn and Ramalingam 2012). This led to the hypothesis that a possible anti-fibrotic target point might lay in the inhibition of proliferation.

To verify already described anti-proliferative properties of pirfenidone in rat cardiac fibroblasts (Shi Q et al. 2011), a proliferation assay was performed using hCF in 2D cultures. Therefore, the cells were exposed to different concentrations of pirfenidone, and the exposure was carried out for 0, 2 and 4 days to evaluate the dynamic of the cell number.

In line with other studies (Shi Q et al. 2011; Kadir et al. 2016; Cui et al. 2020), pirfenidone inhibited the proliferation of the hCF in a time- and concentration-dependent manner. Concentrations of 0.1 mg/ml and 0.3 mg/ml resulted in a relevant decline in the proliferation rate already on day 2 and became even more pronounced on day 4 compared to the untreated control group. Interestingly, treatment with 1.0 mg/ml pirfenidone did not change the initial seeded cell number within 4 days, which indicates that the cells either got arrested or cell growth and cell death were balanced. The last treatment group was incubated with 3.0 mg/ml pirfenidone, which led to a substantial decrease in cell number on day 2. This indicates that cell death occurred in this condition. Therefore, concentrations above 1.0 mg/ml were omitted in all further experiments. In general, the observed effects of pirfenidone on the proliferation of hCF are in line with other studies using fibroblasts from the human lung (Conte et al. 2014), the intestines (Sun et al. 2018; Cui et al. 2020), or epidural scars (Shi et al. 2019). Kadir et al. (2016) even demonstrated that pirfenidone inhibited proliferation of gut-derived fibroblasts regardless of their origin from inflamed or non-inflamed mucosa. Additionally, also non-fibroblast cells, like mesothelioma cells, showed a significantly reduced proliferation after pirfenidone treatment (Li et al. 2018). Similar, in this study pirfenidone inhibited the proliferation of immortalized human embryonic kidney cells (tsA201). However, the effective concentration was higher as for hCF, also reflected by the higher IC_{50} value (0.43 mg/ml for hCF vs. 0.71 mg/ml for ttsA201 cells), as well as compared to the effective published concentration of 0.25 mg/ml for mesothelioma cells (Li et al. 2018). In fact, at least 1.0 mg/ml pirfenidone was necessary to significantly inhibit the proliferation of tsA201 cells. Whether the reduced sensitivity of tsA201 cells for pirfenidone is dependent on their extreme high proliferation rate or their immortalized nature of the cells, is currently unknown.

As mentioned above, a stagnation in cell number could result either from a cellular arrest or an imbalance between cell growth and death. Therefore, it was necessary to evaluate if pirfenidone caused cytotoxic side effects or influenced pro-proliferative molecular pathways. As described above, the highest concentration of 3 mg/ml was excluded from all following investigations, thus, the cells were treated with 0, 0.1, 0.3, and 1.0 mg/ml pirfenidone for 48 h. This time, the cells were treated when they reached confluency. After the treatment, live staining was performed using Hoechst33342 and propidium iodide. The DNA dye Hoechst33342 was used to count all cells and propidium iodide was added to label dying or dead cells, as it is only permeant to a disrupted plasma membrane (Atale et al. 2014). The analysis demonstrated that under these conditions no cytotoxic side effects were observed regardless of the used concentration of pirfenidone.

These findings are in line with the results presented by Shi and colleagues (Shi Q et al. 2011), who assessed the effect of pirfenidone in rat cardiac fibroblasts using a tryptan blue exclusion test and measuring the release of lactate dehydrogenase. Additionally, further studies on human fibroblasts, derived from the intestines, epidural scars, or the lung, did not detect any cytotoxic or apoptotic effects using dosages between 0- 1.5 mg/ml (Shi Q et al. 2011; Conte et al. 2014; Sun et al. 2018; Shi et al. 2019). Moreover, Cui et al. 2020 treated human intestinal fibroblasts for 72 h with 2.0 mg/ml pirfenidone and less than 1% of the cells were necrotic and there was no increase in apoptosis. Taken together, these findings strongly indicate that pirfenidone exert its anti-proliferative effects on hCF in concentrations equals or lower than 1 mg/ml in a non-cytotoxic manner. This hypothesis is also backed up by the findings of Kadir and colleagues, which proved that the proliferation rate normalized after the removal of pirfenidone from the medium (Kadir et al. 2016). Hence, it must be assumed that the observed effects are due to partly reversible changes of intracellular signalling pathways.

After ruling out direct cytotoxic effects, changes in the cell shape following pirfenidone treatment using 0, 0.1, 0.3, and 1.0 mg/ml were evaluated by staining with DAPI, WGA-Alexa Fluor 488, and TRITC-phalloidin and imaged using a fluorescence microscope. Except the visible decrease in total cell number, there were no striking differences in terms of actin fibre formation and glycosylation. Additionally, the nuclear shape stayed unaffected further supporting the absence of enhanced cell death. These findings match with other studies investigating the morphology of human intestinal fibroblasts after incubation with pirfenidone (Cui et al. 2020).

4.2 Pirfenidone and TGF-β1 signalling

In the pathogenesis of fibrosis, the growth factor TGF-β is known to be a crucial player. By activating several downstream pathways, the cytokine induces fibroblast activation and differentiation into myofibroblasts, which represents one of the major events during fibrogenesis. The cells start to deposit more and more extracellular matrix proteins, like collagen type I and III, resulting in fibrotic remodelling. Hence, TGF-β activation, for example by hormonal signalling like the renin-angiotensin-aldosterone system or increased oxidative stress, is one of the main pathways leading to cardiac fibrosis (Aimo et al. 2021).

Given its central role in the development of fibrosis, the possible impact of pirfenidone on the TGF-β signalling pathways was subject to many investigations. A previous study by Shi and colleagues provided evidence that pirfenidone could decrease TGF-β 1 transcription in cardiac fibroblasts, even after treatment with angiotensin II (Shi Q et al. 2011). Furthermore, Cui et al. (2020) showed that pirfenidone treatment significantly decreased the TGF-β1-induced

expression of collagen I in intestinal fibroblasts not only at protein, but also on mRNA level. Additionally, pirfenidone also countervailed the TGF-β-induced fibroblast proliferation and apoptosis prevention (Sun et al. 2018; Shi et al. 2019).

On a molecular level, previous studies indicated that TGF-β mediates the activation of quiescent cardiac fibroblasts through the canonical signalling via SMAD2 and SMAD3 transcription factors as they proved that the deletion of SMAD2/3 decreased the fibrotic response (Khalil et al. 2017). In this context, it was of interest if pirfenidone interferes with SMAD activation in hCF. Therefore, the cells were pre-incubated with different pirfenidone concentrations for 4 h and subsequently treated with 5 ng/ml TGF-β1 for 30 min. The phosphorylation status of SMAD2 and SMAD3 were analysed. As expected, and already described by previous studies, phosphorylated SMAD2 and SMAD3 levels were increased in the presence of TGF-β1 (Hu et al. 2018). Importantly, pirfenidone treatment reduced the amount of phosphorylated SMAD2, but not of SMAD3, only in the presence of TGF-β1. These findings bear similarities to other investigations. Shi et al. (2019) demonstrated that pirfenidone reduced SMAD2 and SMAD3 phosphorylation in epidural scar fibroblast after 48 h of incubation with 5 ng/ml TGF-β1 together with different concentrations of pirfenidone. Sun et al. (2018) pre-incubated human intestinal fibroblasts for 1 h with 1 mg/ml pirfenidone, afterwards 10 ng/ml TGF-β1 was added for 48 h and a significant reduction of TGF-β-induced SMAD2/3-phosphorylation was found. In contrast, Cui et al. (2020) exposed intestinal fibroblasts for 6 h with 2.5 ng/ml TGF-β1 and 1 mg/ml pirfenidone, which did not lead to any relevant change in SMAD2/3 phosphorylation. These discrepancies might result from the different experimental set ups. TGF-β signalling is thought to be dependent on the number of TGF-β molecules per cell and not on the applied concentration. Moreover, the number of molecules determines the response type, which can be a graded short-term response or a switch-like long-term response. A mature determinant thereby is the phosphorylation level of SMAD2, which is fully transient at low TGF-β/cell ratios and sustained when the TGF-β/cell ratio is high. It is important to mention that also the sustained response displays in the beginning a peak in SMAD2 phosphorylation, which occurs within the first 45 min after TGF-β application (Zi et al. 2012). Based on this, one can conclude that the other mentioned studies mainly analyzed the sustained reaction, whereas in this thesis the first peak in SMAD2 phosphorylation was investigated.

Besides the canonical signalling via SMADs, TGF-β is known to exert its effect through further non-canonical pathways like the ERK1/2-MAPK pathway which includes the phosphorylation of several kinases like Raf, MEK1/2, and eventually ERK1/2. Besides, activated ERK1/2 also contributes to the phosphorylation of SMADs as part of multiple cross-talks between the different pathways (Tzavlaki and Moustakas 2020). Similar as for the canonical TGF-β

signalling, MAPK activation has been demonstrated to play a central role in mediating cardiac hypertrophy and fibrogenesis (Ma et al. 2017; Kumar et al. 2019).

To investigate if pirfenidone might exert its effect additionally through the non-canonical TGF-β1 signalling, the influence of pirfenidone on the phosphorylation status of MAPK ERK1/2 was tested. Unexpectedly, TGF-β1 elicited no effect after 30 min. In contrast, pirfenidone reduced the amount of phosphorylated ERK1/2 in a concentration-dependent manner in the presence and absence of TGF-β1. These findings are in line with results from Guo et al. (2017), who found out that pirfenidone concentrations of 0.3 and 0.6 mg/ml significantly reduced ERK1/2 phosphorylation in a similar concentration-dependent manner in human tendon fibroblasts. Shorter periods of treatment appear to be insufficient to exert significant effects, as Choi et al. (2012) could not detect a decrease in ERK1/2 phosphorylation under basal conditions and in the presence of TGF-β1 after 1 h of pre-incubation with 0.5 mg/ml pirfenidone in retinal pigment epithelial cells.

Kinases upstream of ERK1/2 are MEK1/2, which were analysed in addition. Similarly, as found for ERK1/2, MEK1/2 phosphorylation was decreased in the presence of pirfenidone in both, TGF-β stimulated and unstimulated, settings. In fact, the inhibitory effect of pirfenidone was more pronounced in case of MEK1/2 phosphorylation, which indicates that pirfenidone might indeed act up-stream of ERK1/2. The MEK1/2-ERK1/2 signalling axis, seem to be, however, not the only relevant kinase pathways. Other studies demonstrated that pirfenidone also influences Akt und p38 phosphorylation in the presence of TGF-β, however, without investigating its effect in the absence of it (Conte et al. 2014; Shi et al. 2019), and there is data on carpal tunnel fibroblasts showing that pirfenidone alone is sufficient to reduce the phosphorylation of Akt and p38 (Zhou et al. 2019).

Taken together, the obtained 2D data suggests that pirfenidone inhibits hCF proliferation without relevant cytotoxic effects at concentrations of 1 mg/ml or below. A likely explanation for its anti-proliferative effect could lay in the inhibition of the mitogenic MEK1/2-ERK1/2 signalling pathway.

4.3 Pirfenidone does not lower the oxidative effect of H_2O_2

Oxidative stress and especially the generation of reactive oxygen species (ROS) are known to be important parameters in the development of cardiac hypertrophy and fibrogenesis. Elevated levels of ROS or other oxidants lead to either direct cellular damage through nonspecific oxidation of lipids or DNA, or through activation of transcription factors like NF-κB or an increased production of TGF-β, inducing proliferation and cardiac remodelling (Gaspar-Pereira et al. 2012; Purnomo et al. 2013).

Previous studies suggested that pirfenidone might exert its anti-fibrotic effect partly through a reduction in ROS production and prevention of oxidative stress (Ruwanpura et al. 2020). To reproduce these observations, tsA201 cells stably expressing a redox sensor called HyPer were pre-treated with 0 or 1 mg/ml pirfenidone. As an oxidant reagent H_2O_2 was used and different dilutions were added while measuring the changes in fluorescence. Interestingly, the pirfenidone-treated cells showed a contrary behaviour compared to the expectations. The oxidative state induced by the addition of H_2O_2 seemed to be stabilized in the pirfenidone treated cells, whereas the control group showed a trend to re-establish the normally reductive cytoplasmatic environment. The reason for these unexpected results might be caused by the short pre-treatment of 4 h, as Monsalvo-Villegas et al. (2018) proved that a minimum of 8 h pirfenidone treatment is necessary to observe anti-oxidative effects. They also showed a decreased ROS production in pirfenidone treated cardiac myocytes after a 30 min exposure to H_2O_2. These findings indicate that pirfenidone exerts its effects through more long-term interactions and the experimental setting should include longer periods of incubation and measuring.

4.4 Pirfenidone influences the morphology and biomechanical properties of ECT

To specifically address the impact of pirfenidone on hCF in a more *in vivo*-like environment, this study used the ECT model consisting of cultured hCF and collagen I. The model give rise to ring-shaped tissues and exists in two distinct mechanical conditions given by the geometry of the moulds. The ring shape allows to analyse the dimensions of the ECT and more importantly the biomechanical properties as destructive tensile strength measurements can be easily performed using a dynamic mechanical analyzer with two custom-made hooks on which the ECT are placed. The varying mould geometries, which were equipped with two flexible poles or a central stiff rod, have been demonstrated to result in tissues with stiffnesses similar to the healthy and diseased heart (Pislaru et al. 2014; Santos Rer. nat. Diss. Göttingen 2021). In line, the ECT generated in this thesis displayed under control conditions stiffnesses of around 20 kPa in the flexible model and 75 kPa in the stiff model. Moreover, the herein presented data further support the previous finding that stiff ECT are more compact and less elastic and extensible (Santos Rer. nat. Diss. Göttingen 2021).

To test the effect of pirfenidone, 1 h after ECT generation 0, 0.3, or 1.0 mg/ml pirfenidone was added to the medium. The ECT were treated for 5 days and their shape was documented. As already visible on a macroscopic level, the measured CSA of the treated tissues were significantly increased after 5 days in both models, indicating that the perpendicular contractile ability of the

embedded cells was reduced. This was accompanied by an impaired longitudinal contraction in the presence of 1 mg/ml pirfenidone in the flexible model. Similar to this study, Tao et al. (2020) demonstrated that pirfenidone inhibited the collagen contraction of embedded pterygium fibroblasts with a delayed of 3 days. However, Wells and Leung (2020) demonstrated that the anti-contractile effects of pirfenidone on TGF-β1-pretreated dermal fibroblasts constructs were detectable already after 1 day of treatment. Their data further suggested, as demonstrated with 2D cultures, that a down-regulation in α-smooth muscle actin in the myofibroblasts could serve as an explanation for the contractile impairing effect of pirfenidone, but no data was provided with 3D-cultured cells.

As the impaired contraction occurred with a certain delay in this study, it was hypothesized that either a cell loss or disturbances in the contractile machinery of the cells, which might manifests not immediately, could be responsible. Therefore, the number and viability of cells in the respective ECT were analysed. First of all, a general loss of cells under control conditions in both models was observed after re-isolation, which is in line with former results of our group (Santos Rer. nat. Diss. Göttingen 2021). Furthermore, it was shown before that the number of fibroblasts in 3D constructs decreases when the initially used number is above the percolation threshold, which is the cell number necessary for the formation of a steric cell network (Marquez et al. 2006). In addition, the technical process might not allow for an isolation of all cells and could impair the viability of the isolated cells. A comparison of the cell number and viability of the two models indicated that under control conditions more cells with a higher viability were isolated from the stiff compared to flexible ECT as demonstrated before (Santos Rer. nat. Diss. Göttingen 2021).

The treatment with the lower pirfenidone concentration did not affect the cell numbers and viabilities compared to the control group. However, the higher concentration led to a substantial loss of viable cells in both models and the effect was slightly more pronounced in the flexible model. To gain further insight in this process, a cell cycle analysis was performed. Thereby it was found that 1 mg/ml pirfenidone increased the percentages of cells in G0/G1-phase and accordingly decreased them in S- and G2/M-phases in both models, indicating that the cell cycle activity is reduced in the presence of pirfenidone. Equal results were demonstrated by previous studies, which also indicated that the G1 arrest might be by suppression of the expression of crucial kinases, like CDK2 or CDK6, as a consequence of a dysregulated ERK1/2 and TGF-β signalling (Conte et al. 2014; Guo et al. 2017; Tao et al. 2020). Taken together, the obtained data demonstrates that pirfenidone negatively influences the balance between the percolation threshold-dependent cell loss and the residual cell cycle activity of the embedded hCF in the ECT model, resulting in a netto cell reduction. This reduction could well explain the observed

effects on ECT compaction and contraction. Furthermore, it could serve as an explanation for the differences in the biomechanical properties of the ECT as determined by the destructive tensile strength measurements.

Only the treatment with 1 mg/ml pirfenidone demonstrated significant effects on the biomechanical properties in both ECT models. It reduced the stiffnesses in both models and in addition the ultimate strain in the stiff model. Moreover, the stiff ECT displayed an enhanced elasticity and extensibility compared to control. As it was show before that the hCF in the stiff model express higher levels of myofibroblast markers and resemble an ECM signature of the fibrotic heart (Santos Rer. nat. Diss. Göttingen 2021), it can be concluded that pirfenidone might affect cells more effectively under fibrotic conditions. This is in line with data obtained with engineered human lung microtissues, by which it was shown that pirfenidone decreased tissue contractility and stiffness, and increased the tissue compliance in a fibrotic environment (Asmani et al. 2018).

4.5 Conclusion and future prospect

In this study it was demonstrated that pirfenidone is able to influence the contractile behaviour of 3D-cultured hCF and the biomechanical properties of the corresponding tissues. Especially, the effects on the biomechanical properties were more pronounced in a more fibrotic environment, leading to the conclusion that it could exert beneficial effects in the treatment of cardiac fibrosis. Although the exact mechanism of action remain undisclosed, interferences with cell proliferation and cell cycle activity by inhibition of the TGF-β and MAPK signalling could serve as possible explanations for these findings. First published results from the PIROUETTE trial indeed demonstrated that pirfenidone can significantly reduce the myocardial extracellular volume in patients with HFpEF (Lewis et al. 2021). However, the enhanced observed cell loss in ECT, independent of the mechanical condition, might argue that pirfenidone should not be applied when reparative fibrosis is necessary.

Further aspects of interest should lay in the question if the effects of pirfenidone are reversible after termination of the treatment. In addition, it should be assessed if a prolonged treatment with a lower concentration might exert the same beneficial effects on the tissue properties without inducing cell loss. It is also questionable, if a delayed treatment with pirfenidone is still able to change the stiffness of the tissues, because, so far, this study only proved how it interferes with the development of fibrosis, but not if it is able to reverse the process. Additionally, other cell types should be included into the 3D model. Eventually, the mechanism how pirfenidone exert its effects should be investigated further, as the knowledge of the exact target provides a rational usage in the medicine. So far, only basal data about many different pathways besides

the TGF-β signalling are available. Hence, pirfenidone was also proven to influence growth factors like platelet-derived growth factor, matrix metalloproteinases or even components of the immune system, which makes it a versatile tool for the future treatment of several other diseases (Hu et al. 2018; Li et al. 2018; Lv et al. 2020; Ruwanpura et al. 2020). In fact, latest studies even suggested pirfenidone as a potential new treatment for COVID-19 (Seifirad 2020). At present, pirfenidone is subject of many ongoing preclinical trials, its benefits for the treatment of the idiopathic pulmonary fibrosis have been proven many times. However, current trials concerning other diseases are still ongoing or are not published, so far (Shah et al.). Thus, the real impact of pirfenidone as a new anti-fibrotic drug remains a subject to future studies.

5. Summary

Even after years of investigations cardiac fibrosis remains a poorly understood event in the framework of several pathological heart conditions eventually leading to heart failure. One major problem lays in the lack of an effective and target-oriented therapy. The promising drug pirfenidone is a small synthetic molecule that proved its effectiveness in the treatment of pulmonary fibrosis and is currently in clinical testing for the treatment of patients with heart failure with preserved ejection fraction. Therefore, the aim of this study was to investigate if and in what extent pirfenidone exerts anti-fibrotic effects on cardiac fibroblasts, the major driver of cardiac fibrosis.

First, analysis of 2D human cardiac fibroblasts cultures showed that pirfenidone inhibits cell proliferation in a time- and concentration-dependent manner, without exerting obvious effects on cell morphology.

To compare the effects to a different cell line, immortalized human embryonic kidney cells (tsA201) were used and a similar, but less potent inhibition of cell proliferation was observed. Further, pirfenidone did not exert cytotoxic effects, when applied to confluent cardiac fibroblasts cultures.

Mechanistically, pirfenidone inhibited the TGF-β-induced SMAD2 phosphorylation as well as the phosphorylation of the mitogenic kinases ERK1/2 and MEK1/2.

Previous studies suggested that pirfenidones might exert antifibrotic effects through the reduction of reactive oxygen species. In this study, tsA201 cells, which stably expressed the H_2O_2 sensor HyPer, were treated with pirfenidone and no influence on the basal sensor oxidation could be detected, but surprisingly after H_2O_2 application the sensor displayed in the presence of pirfenidone a prolonged oxidation.

In the second part of the thesis, the effect of pirfenidone was tested in 3D cultures of human cardiac fibroblasts under different mechanical constraints. Under basal conditions, low and high mechanical stress resulted in engineered connective tissues (ECT) with stiffness reflecting those of the healthy and diseased myocardium. Moreover, high mechanical stress induced an enhanced compaction and a reduced elasticity and extensibilities of the ECT compared to low mechanical stress.

Pirfenidone treatment impaired the contraction in the low mechanical stress model and the compaction of the ECT in both models. Moreover, pirfenidone reduced the ECT stiffness in both models and the elasticity and extensibility under high mechanical stress. Cell analysis demonstrated that the cell number and viability as well as the cell cycle activity is reduced in the presence of pirfenidone independent of the used model.

In summary, this study showed that pirfenidone induces anti-fibrotic effects in cardiac fibroblasts in 2D and 3D models. These findings indicate that pirfenidone might act as a novel approach for the treatment of cardiac fibrosis.

6. Bibliography

Aimo A, Cerbai E, Bartolucci G, Adamo L, Barison A, Lo Surdo G, Biagini S, Passino C, Emdin M (2020): Pirfenidone is a cardioprotective drug: Mechanisms of action and preclinical evidence. Pharmacol Res 155, 104694

Aimo A, Spitaleri G, Panichella G, Lupón J, Emdin M, Bayes-Genis A (2021): Pirfenidone as a novel cardiac protective treatment. Heart Fail Rev, 525–532

Asmani M, Velumani S, Li Y, Wawrzyniak N, Hsia I, Chen Z, Hinz B, Zhao R (2018): Fibrotic microtissue array to predict anti-fibrosis drug efficacy. Nat Commun 9, 2066

Atale N, Gupta S, Yadav UCS, Rani V (2014): Cell-death assessment by fluorescent and nonfluorescent cytosolic and nuclear staining techniques. J Microsc 255, 7–19

Baranyi U, Winter B, Gugerell A, Hegedus B, Brostjan C, Laufer G, Messner B (2019): Primary Human Fibroblasts in Culture Switch to a Myofibroblast-Like Phenotype Independently of TGF Beta. Cells 8, 721

Barocas VH, Moon AG, Tranquillo RT (1995): The fibroblast-populated collagen microsphere assay of cell traction force--Part 2: Measurement of the cell traction parameter. J Biomech Eng 117, 161–170

Belousov VV, Fradkov AF, Lukyanov KA, Staroverov DB, Shakhbazov KS, Terskikh AV, Lukyanov S (2006): Genetically encoded fluorescent indicator for intracellular hydrogen peroxide. Nat Methods 3, 281–286

Bracco Gartner TCL, Deddens JC, Mol EA, Magin Ferrer M, van Laake LW, Bouten CVC, Khademhosseini A, Doevendans PA, Suyker WJL, Sluijter JPG, Hjortnaes J (2019): Anti-fibrotic Effects of Cardiac Progenitor Cells in a 3D-Model of Human Cardiac Fibrosis. Front Cardiovasc Med 6, 52

Cano ML, Cassimeris L, Joyce M, Zigmond SH (1992): Characterization of tetramethylrhodaminyl-phalloidin binding to cellular F-actin. Cell Motil Cytoskeleton 21, 147–158

Carthy JM (2018): TGFβ signaling and the control of myofibroblast differentiation: Implications for chronic inflammatory disorders. J Cell Physiol 233, 98–106

Chan MWC, Hinz B, McCulloch CA (2010): Mechanical induction of gene expression in connective tissue cells. Methods Cell Biol 98, 178–205

Chao J, Dai X, Peña T, Doyle DA, Guenther TM, Carlson MA (2015): MCPIP1 regulates fibroblast migration in 3D collagen matrices downstream of MAP kinases and NF-ϰB. J Invest Dermatol 135, 2944–2954

Chazotte B (2011): Labeling Membrane Glycoproteins or Glycolipids with Fluorescent Wheat Germ Agglutinin. Cold Spring Harb Protoc 2011, pdb.prot5623-pdb.prot5623

Chen H, Moreno-Moral A, Pesce F, Devapragash N, Mancini M, Heng EL, Rotival M, Srivastava PK, Harmston N, Shkura K, et al. (2019): WWP2 regulates pathological cardiac fibrosis by modulating SMAD2 signaling. Nat Commun. 2019; 10: 4085.

Cho N, Razipour SE, McCain ML (2018): Featured Article: TGF-β1 dominates extracellular matrix rigidity for inducing differentiation of human cardiac fibroblasts to myofibroblasts. Exp Biol Med 243, 601–612

Choi K, Lee K, Ryu S W, Im M, Kook KH, Choi C (2012): Pirfenidone inhibits transforming growth factor-β1-induced fibrogenesis by blocking nuclear translocation of Smads in human retinal pigment epithelial cell line ARPE-19. Mol Vis 18, 1010–1020

Conte E, Gili E, Fagone E, Fruciano M, Iemmolo M, Vancheri C (2014): Effect of pirfenidone on proliferation, TGF-β-induced myofibroblast differentiation and fibrogenic activity of primary human lung fibroblasts. Eur J Pharm Sci 58, 13–19

Cui Y, Zhang M, Leng C, Blokzijl T, Jansen BH, Dijkstra G, Faber KN (2020): Pirfenidone Inhibits Cell Proliferation and Collagen I Production of Primary Human Intestinal Fibroblasts. Cells 9 (3):775

Dallon JC, Ehrlich HP (2008): A review of fibroblast-populated collagen lattices. Wound Repair Regen Off Publ Wound Heal Soc Eur Tissue Repair Soc 16, 472–479

de Boer RA, De Keulenaer G, Bauersachs J, Brutsaert D, Cleland JG, Diez J, Du X, Ford P, Heinzel FR, Lipson KE, et al. (2019): Towards better definition, quantification and treatment of fibrosis in heart failure. A scientific roadmap by the Committee of Translational Research of the Heart Failure Association (HFA) of the European Society of Cardiology. Eur J Heart Fail 21, 272–285

Derynck R, Zhang YE (2003): Smad-dependent and Smad-independent pathways in TGF-b family signalling. Nature 425, 577–584

Eastwood M, Porter R, Khan U, McGrouther G, Brown R (1996): Quantitative analysis of collagen gel contractile forces generated by dermal fibroblasts and the relationship to cell morphology. J Cell Physiol 166, 33–42

Elson EL, Genin GM (2016): Tissue constructs: platforms for basic research and drug discovery. Interface Focus. 6. 20150095.20150095

Espeland T, Lunde IG, Amundsen BH, Gullestad L, Aakhus S (2018): Myocardial fibrosis. Tidsskr Den Nor Legeforening 12;138(16)

Fang L, Murphy AJ, Dart AM (2017): A Clinical Perspective of Anti-Fibrotic Therapies for Cardiovascular Disease. Front Pharmacol 8, 186

Galie PA, Westfall MV, Stegemann JP (2011): Reduced serum content and increased matrix stiffness promote the cardiac myofibroblast transition in 3D collagen matrices. Cardiovasc Pathol Off J Soc Cardiovasc Pathol 20, 325–333

Gaspar-Pereira S, Fullard N, Townsend PA, Banks PS, Ellis EL, Fox C, Maxwell AG, Murphy LB, Kirk A, Bauer R, et al. (2012): The NF-κB Subunit c-Rel Stimulates Cardiac Hypertrophy and Fibrosis. Am J Pathol 180, 929–939

González A, Schelbert EB, Díez J, Butler J (2018): Myocardial Interstitial Fibrosis in Heart Failure: Biological and Translational Perspectives. J Am Coll Cardiol 71, 1696–1706

Gourdie RG, Dimmeler S, Kohl P (2016): Novel therapeutic strategies targeting fibroblasts and fibrosis in heart disease. Nat Rev Drug Discov 15, 620–638

Graziani F, Varone F, Crea F, Richeldi L (2018): Treating heart failure with preserved ejection fraction: learning from pulmonary fibrosis. Eur J Heart Fail 20(10):1385-1391.

Guo X, Yang Y, Liu L, Liu X, Xu J, Wu K, Yu M (2017): Pirfenidone Induces G1 Arrest in Human Tenon's Fibroblasts In Vitro Involving AKT and MAPK Signaling Pathways. J Ocul Pharmacol Ther Off J Assoc Ocul Pharmacol Ther 33, 366–374

Hartmann S: Modulation of Cardiac Fibroblast to Myofibroblast Transition by Rho-Associated Kinases ROCK1 and ROCK2. Mol. Med. Diss. Göttingen 2016

Hernández-Barrera A, Quinto C, Johnson EA, Wu H-M, Cheung AY, Cárdenas L (2013): Using hyper as a molecular probe to visualize hydrogen peroxide in living plant cells: a method with virtually unlimited potential in plant biology. Methods Enzymol 527, 275–290

Hisatomi K, Mukae H, Sakamoto N, Ishimatsu Y, Kakugawa T, Hara S, Fujita H, Nakamichi S, Oku H, Urata Y, et al. (2012): Pirfenidone inhibits TGF-β1-induced over-expression of collagen type I and heat shock protein 47 in A549 cells. BMC Pulm Med 12, 24

Hu H-H, Chen D-Q, Wang Y-N, Feng Y-L, Cao G, Vaziri ND, Zhao Y-Y (2018): New insights into TGF-β/Smad signaling in tissue fibrosis. Chem Biol Interact 292, 76–83

Ivey MJ, Tallquist MD (2016): Defining the Cardiac Fibroblast. Circ J Off J Jpn Circ Soc 80, 2269–2276

Iyer SN, Gurujeyalakshmi G, Giri SN (1999): Effects of pirfenidone on transforming growth factor-beta gene expression at the transcriptional level in bleomycin hamster model of lung fibrosis. J Pharmacol Exp Ther 291, 367–373

Kadir S-I, Wenzel Kragstrup T, Dige A, Kok Jensen S, Dahlerup JF, Kelsen J (2016): Pirfenidone inhibits the proliferation of fibroblasts from patients with active Crohn's disease. Scand J Gastroenterol 51, 1321–1325

Khalil H, Kanisicak O, Prasad V, Correll RN, Fu X, Schips T, Vagnozzi RJ, Liu R, Huynh T, Lee S-J, et al. (2017): Fibroblast-specific TGF-β–Smad2/3 signaling underlies cardiac fibrosis. J Clin Invest 127, 3770–3783

Kong P, Christia P, Frangogiannis NG (2014): The Pathogenesis of Cardiac Fibrosis. Cell Mol Life Sci CMLS 71, 549–574

Kong P, Shinde AV, Su Y, Russo I, Chen B, Saxena A, Conway SJ, Graff JM, Frangogiannis NG (2018): Opposing actions of fibroblast and cardiomyocyte Smad3 signaling in the infarcted myocardium. Circulation 137, 707–724

Kumar S, Wang G, Zheng N, Cheng W, Ouyang K, Lin H, Liao Y, Liu J (2019): HIMF (Hypoxia-Induced Mitogenic Factor)-IL (Interleukin)-6 Signaling Mediates Cardiomyocyte-Fibroblast Crosstalk to Promote Cardiac Hypertrophy and Fibrosis. Hypertension 73, 1058–1070

Kuwahara F, Kai H, Tokuda K, Kai M, Takeshita A, Egashira K, Imaizumi T (2002): Transforming growth factor-beta function blocking prevents myocardial fibrosis and diastolic dysfunction in pressure-overloaded rats. Circulation 106, 130–135

Lewis GA, Schelbert EB, Naish JH, Bedson E, Dodd S, Eccleson H, Clayton D, Jimenez BD, McDonagh T, Williams SG, et al. (2019): Pirfenidone in Heart Failure with Preserved Ejection Fraction—Rationale and Design of the PIROUETTE Trial. Cardiovasc Drugs Ther 33, 461–470

Lewis GA, Dodd S, Clayton D, Bedson E, Eccleson H, Schelbert EB, Naish JH, Jimenez BD, Williams SG, Cunnington C, et al. (2021): Pirfenidone in heart failure with preserved ejection fraction: a randomized phase 2 trial. Nat Med 27, 1477–1482

Li C, Rezov V, Joensuu E, Vartiainen V, Rönty M, Yin M, Myllärniemi M, Koli K (2018): Pirfenidone decreases mesothelioma cell proliferation and migration via inhibition of ERK and AKT and regulates mesothelioma tumor microenvironment in vivo. Sci Rep 8, 10070

Lin X, Yu M, Wu K, Yuan H, Zhong H (2009): Effects of Pirfenidone on Proliferation, Migration, and Collagen Contraction of Human Tenon's Fibroblasts In Vitro. Invest Ophthalmol Vis Sci 50, 3763–3770

Litviňuková M, Talavera-López C, Maatz H, Reichart D, Worth CL, Lindberg EL, Kanda M, Polanski K, Heinig M, Lee M, et al. (2020): Cells of the adult human heart. Nature 588, 466–472

Lopez-de la Mora DA, Sanchez-Roque C, Montoya-Buelna M, Sanchez-Enriquez S, Lucano-Landeros S, Macias-Barragan J, Armendariz-Borunda J (2015): Role and New Insights of Pirfenidone in Fibrotic Diseases. Int J Med Sci 12, 840–847

Lucas JA, Zhang Y, Li P, Gong K, Miller AP, Hassan E, Hage F, Xing D, Wells B, Oparil S, Chen Y-F (2010): Inhibition of transforming growth factor-β signaling induces left ventricular dilation and dysfunction in the pressure-overloaded heart. Am J Physiol - Heart Circ Physiol 298, H424–H432

Lv Q, Wang J, Xu C, Huang X, Ruan Z, Dai Y (2020): Pirfenidone alleviates pulmonary fibrosis in vitro and in vivo through regulating Wnt/GSK-3β/β-catenin and TGF-β1/Smad2/3 signaling pathways. Mol Med 26, 49

Ma Z-G, Yuan Y-P, Zhang X, Xu S-C, Wang S-S, Tang Q-Z (2017): Piperine Attenuates Pathological Cardiac Fibrosis Via PPAR-γ/AKT Pathways. EBioMedicine 18, 179–187

Ma Z-G, Yuan Y-P, Wu H-M, Zhang X, Tang Q-Z (2018): Cardiac fibrosis: new insights into the pathogenesis. Int J Biol Sci 14, 1645–1657

Markvicheva KN, Bilan DS, Mishina NM, Gorokhovatsky AY, Vinokurov LM, Lukyanov S, Belousov VV (2011): A genetically encoded sensor for H2O2 with expanded dynamic range. Bioorg Med Chem 19, 1079–1084

Marquez JP, Genin GM, Pryse KM, Elson EL (2006): Cellular and Matrix Contributions to Tissue Construct Stiffness Increase with Cellular Concentration. Ann Biomed Eng 34, 1475–1482

Martinez FJ, Collard HR, Pardo A, Raghu G, Richeldi L, Selman M, Swigris JJ, Taniguchi H, Wells AU (2017): Idiopathic pulmonary fibrosis. Nat Rev Dis Primer 3, 17074

Meyer KC, Decker CA (2017): Role of pirfenidone in the management of pulmonary fibrosis. Ther Clin Risk Manag 13, 427–437

Misra HP, Rabideau C (2000): Pirfenidone inhibits NADPH-dependent microsomal lipid peroxidation and scavenges hydroxyl radicals. Mol Cell Biochem 204, 119–126

Mitani Y, Sato K, Muramoto Y, Karakawa T, Kitamado M, Iwanaga T, Nabeshima T, Maruyama K, Nakagawa K, Ishida K, Sasamoto K (2008): Superoxide scavenging activity of pirfenidone-iron complex. Biochem Biophys Res Commun 372, 19–23

Monsalvo-Villegas A, Osornio-Garduño DS, Avila G (2018): Long-Term Regulation of Excitation-Contraction Coupling and Oxidative Stress in Cardiac Myocytes by Pirfenidone. Front Physiol 9, 1801

Moore-Morris T, Guimarães-Camboa N, Banerjee I, Zambon AC, Kisseleva T, Velayoudon A, Stallcup WB, Gu Y, Dalton ND, Cedenilla M, et al. (2014): Resident fibroblast lineages mediate pressure overload–induced cardiac fibrosis. J Clin Invest 124, 2921–2934

Mügge F: The role of tubulin acetylation in cardiac fibroblasts. Med. Diss. Göttingen 2018

Niethammer P, Grabher C, Look AT, Mitchison TJ (2009): A tissue-scale gradient of hydrogen peroxide mediates rapid wound detection in zebrafish. Nature 459, 996–999

Ogura T, Taniguchi H, Azuma A, Inoue Y, Kondoh Y, Hasegawa Y, Bando M, Abe S, Mochizuki Y, Chida K, et al. (2015): Safety and pharmacokinetics of nintedanib and pirfenidone in idiopathic pulmonary fibrosis. Eur Respir J 45, 1382–1392

Okamura K, Nakagama Y, Takeda N, Soma K, Sato T, Isagawa T, Kido Y, Sakamoto M, Manabe I, Hirata Y, et al. (2019): Therapeutic targeting of mitochondrial ROS ameliorates murine model of volume overload cardiomyopathy. J Pharmacol Sci 141, 56–63

Oyamada S, Bianchi C, Takai S, Chu LM, Sellke FW (2011): Chymase Inhibition Reduces Infarction and Matrix Metalloproteinase-9 Activation and Attenuates Inflammation and Fibrosis after Acute Myocardial Ischemia/Reperfusion. J Pharmacol Exp Ther 339, 143–151

Pan L, Belloni P, Ding HT, Wang J, Rubino CM, Putnam WS (2017): A Pharmacokinetic Bioequivalence Study Comparing Pirfenidone Tablet and Capsule Dosage Forms in Healthy Adult Volunteers. Adv Ther 34, 2071–2082

Park S, Nguyen NB, Pezhouman A, Ardehali R (2019): Cardiac fibrosis: potential therapeutic targets. Transl Res J Lab Clin Med 209, 121–137

Pislaru C, Urban MW, Pislaru SV, Kinnick RR, Greenleaf JF (2014): VISCOELASTIC PROPERTIES OF NORMAL AND INFARCTED MYOCARDIUM MEASURED BY A MULTIFREQUENCY SHEAR WAVE METHOD: COMPARISON WITH PRESSURE-SEGMENT LENGTH METHOD. Ultrasound Med Biol 40, 1785–1795

Pohlers D, Brenmoehl J, Löffler I, Müller CK, Leipner C, Schultze-Mosgau S, Stallmach A, Kinne RW, Wolf G (2009): TGF-β and fibrosis in different organs — molecular pathway imprints. Biochim Biophys Acta BBA - Mol Basis Dis 1792, 746–756

Purnomo Y, Piccart Y, Coenen T, Prihadi JS, Lijnen PJ (2013): Oxidative stress and transforming growth factor-β1-induced cardiac fibrosis. Cardiovasc Hematol Disord Drug Targets 13, 165–172

Qiu Y, Bayomy AF, Gomez MV, Bauer M, Du P, Yang Y, Zhang X, Liao R (2015): A role for matrix stiffness in the regulation of cardiac side population cell function. Am J Physiol Heart Circ Physiol 308, H990-997

Rhee S, Grinnell F (2007): Fibroblast mechanics in 3D collagen matrices. Adv Drug Deliv Rev 59, 1299–1305

Robertson IB, Rifkin DB (2016): Regulation of the Bioavailability of TGF-β and TGF-β-Related Proteins. Cold Spring Harb Perspect Biol. 8(6):a021907.

Rogliani P, Calzetta L, Cavalli F, Matera MG, Cazzola M (2016): Pirfenidone, nintedanib and N-acetylcysteine for the treatment of idiopathic pulmonary fibrosis: A systematic review and meta-analysis. Pulm Pharmacol Ther 40, 95–103

Rog-Zielinska EA, Norris RA, Kohl P, Markwald R (2016): The Living Scar – Cardiac Fibroblasts and the Injured Heart. Trends Mol Med 22, 99–114

Rosenkranz S, Flesch M, Amann K, Haeuseler C, Kilter H, Seeland U, Schlüter K-D, Böhm M (2002): Alterations of beta-adrenergic signaling and cardiac hypertrophy in transgenic mice overexpressing TGF-beta(1). Am J Physiol Heart Circ Physiol 283, H1253-1262

Ruwanpura SM, Thomas BJ, Bardin PG (2020): Pirfenidone: Molecular Mechanisms and Potential Clinical Applications in Lung Disease. Am J Respir Cell Mol Biol 62, 413–422

Sadeghi AH, Shin SR, Deddens JC, Fratta G, Mandla S, Yazdi IK, Prakash G, Antona S, Demarchi D, Buijsrogge MP, et al. (2017): Engineered 3D Cardiac Fibrotic Tissue to Study Fibrotic Remodeling. Advanced healthcare materials, 6(11), 10.1002/adhm.201601434

Santos GL: Mechanical regulation of cardiac fibroblasts. Mol. Med. Diss. Göttingen 2021

Seifirad S (2020): Pirfenidone: A novel hypothetical treatment for COVID-19. Med Hypotheses 144, 110005

Shah PV, Balani P, Lopez AR, Nobleza CMN, Siddiqui M, Khan S A Review of Pirfenidone as an Anti-Fibrotic in Idiopathic Pulmonary Fibrosis and Its Probable Role in Other Diseases. Cureus 13, e12482

Shi K, Wang F, Xia J, Zuo B, Wang Z, Cao X (2019): Pirfenidone inhibits epidural scar fibroblast proliferation and differentiation by regulating TGF-β1-induced Smad-dependent and -independent pathways. Am J Transl Res 11, 1593–1604

Shi Q, Liu X, Bai Y, Cui C, Li J, Li Y, Hu S, Wei Y (2011): In Vitro Effects of Pirfenidone on Cardiac Fibroblasts: Proliferation, Myofibroblast Differentiation, Migration and Cytokine Secretion. PLoS ONE 6

Shi S, Wu Jianhong, Chen Huating, Chen Hui, Wu Jun, Zeng F (2007): Single- and multiple-dose pharmacokinetics of pirfenidone, an antifibrotic agent, in healthy Chinese volunteers. J Clin Pharmacol 47, 1268–1276

Shi X, Qin L, Zhang X, He K, Xiong C, Fang J, Fang X, Zhang Y (2011): Elasticity of cardiac cells on the polymer substrates with different stiffness: an atomic force microscopy study. Phys Chem Chem Phys PCCP 13, 7540–7545

Solon J, Levental I, Sengupta K, Georges PC, Janmey PA (2007): Fibroblast adaptation and stiffness matching to soft elastic substrates. Biophys J 93, 4453–4461

Somogyi V, Chaudhuri N, Torrisi SE, Kahn N, Müller V, Kreuter M (2019): The therapy of idiopathic pulmonary fibrosis: what is next? Eur Respir Rev *28*(153), 190021

Sun Y, Zhang Y, Chi P (2018): Pirfenidone suppresses TGF-β1-induced human intestinal fibroblasts activities by regulating proliferation and apoptosis via the inhibition of the Smad and PI3K/AKT signaling pathway. Mol Med Rep 18, 3907–3913

Tallquist MD, Molkentin JD (2017): Redefining the identity of cardiac fibroblasts. Nat Rev Cardiol 14, 484–491

Tao Y, Chen Q, Zhao C, Yang X, Cun Q, Yang W, Zhang Y, Zhu Y, Zhong H (2020): The in vitro anti-fibrotic effect of Pirfenidone on human pterygium fibroblasts is associated with down-regulation of autocrine TGF-β and MMP-1. Int J Med Sci 17, 734–744

Togami K, Kanehira Y, Tada H (2015): Pharmacokinetic evaluation of tissue distribution of pirfenidone and its metabolites for idiopathic pulmonary fibrosis therapy. Biopharm Drug Dispos 36, 205–215

Toki F, Honkura N, Shirakata Y, Imamura T, Higashiyama S, Nanba D (2013): Second Harmonic Generation Reveals Collagen Fibril Remodeling in Fibroblast-populated Collagen Gels. Cell Struct Funct 38, 229–238

Travers JG, Kamal FA, Robbins J, Yutzey KE, Blaxall BC (2016): Cardiac Fibrosis: The Fibroblast Awakens. Circ Res 118, 1021–1040

Tzavlaki K, Moustakas A (2020): TGF-β Signaling. Biomolecules 10(3), 487

Wakatsuki T, Kolodney MS, Zahalak GI, Elson EL (2000): Cell mechanics studied by a reconstituted model tissue. Biophys J 79, 2353–2368

Weinberger F, Mannhardt I, Eschenhagen T (2017): Engineering Cardiac Muscle Tissue: A Maturating Field of Research. Circ Res 120, 1487–1500

Wynn TA, Ramalingam TR (2012): Mechanisms of fibrosis: therapeutic translation for fibrotic disease. Nat Med 18, 1028–1040

Xiao H, Zhang Y-Y (2008): UNDERSTANDING THE ROLE OF TRANSFORMING GROWTH FACTOR-β SIGNALLING IN THE HEART: OVERVIEW OF STUDIES USING GENETIC MOUSE MODELS. Clin Exp Pharmacol Physiol 35, 335–341

Xie J, Zhang Q, Zhu T, Zhang Y, Liu B, Xu J, Zhao H (2014): Substrate stiffness-regulated matrix metalloproteinase output in myocardial cells and cardiac fibroblasts: implications for myocardial fibrosis. Acta Biomater 10, 2463–2472

Yong KW, Li Y, Huang G, Lu TJ, Safwani WKZW, Pingguan-Murphy B, Xu F (2015): Mechanoregulation of cardiac myofibroblast differentiation: implications for cardiac fibrosis and therapy. Am J Physiol Heart Circ Physiol 309, H532-542

Zhou C, Zeldin Y, Baratz ME, Kathju S, Satish L (2019): Investigating the effects of Pirfenidone on TGF-β1 stimulated non-SMAD signaling pathways in Dupuytren's disease -derived fibroblasts. BMC Musculoskelet Disord 20, 135

Zi Z, Chapnick DA, Liu X (2012): Dynamics of TGF-β/Smad signaling. FEBS Lett 586, 1921–1928

Zuppinger C (2019): 3D Cardiac Cell Culture: A Critical Review of Current Technologies and Applications. Front Cardiovasc Med 6, 87

Acknowledgments

At this point I would like to express my gratitude to everyone who has contributed to this work and supported me throughout the process.

First, I would like to express my deepest thankfulness to Prof. Dr. Susanne Lutz who gave me the opportunity to work in her group and guided me with such patience and encouragement through the steps of this thesis starting with the experimental work, data analysis and finally the writing.

Furthermore, I want to thank the IRTG and especially Dr. Christina Würtz for including me into the program. It was a great experience, not only in a scientific but also in a personal way, to get in touch with so many intelligent and ambitious young scientists.

And of course, many thanks to my lab crew: Gabriela, Alisa, Kristin and Abdul. All of you helped me to navigate through the daily problems of an unexperienced scientist, thank you for never losing your patience with me and making the life in the lab so cheerful and enjoyable.

Also, a sincere thanks to the whole team of the institute for pharmacology and toxicology, for being so friendly and helpful colleagues. And a special thanks to Irina for sharing her HyPer cells with us.